6. Photoelasticity

Photoelasticity is a nondestructive, whole-field, graphic stress-analysis technique based on an opto-mechanical property called *birefringence*, possessed by many transparent polymers.

Combined with other optical elements and illuminated with an ordinary light source, a loaded photoelastic specimen (or photoelastic coating applied to an ordinary specimen) exhibits fringe patterns that are related to the difference between the principal stresses in a plane normal to the light-propagation direction.

The method is used primarily for analyzing two-dimensional plane problems, which is the emphasis in these notes. A method called *stress freezing* allows the method to be extended to three-dimensional problems. Photoelastic coatings are used to analyze surface stresses in bodies of complex geometry.

Advantages and disadvantages

Advantages.—Photoelasticity, as used for two-dimensional plane problems,

- provides reliable full-field values of the difference between the principal normal stresses in the plane of the model
- provides uniquely the value of the non-vanishing principal normal stress along the perimeter(s) of the model, where stresses are generally the largest
- furnishes full-field values of the principal-stress directions (sometimes called stress *trajectories*)
- is adaptable to both static and dynamic investigations
- requires only a modest investment in equipment and materials for ordinary work
- is fairly simple to use

Disadvantages.—On the other hand, photo-elasticity

- requires that a model of the actual part be made (unless photoelastic coatings are used)
- requires rather tedious calculations in order to separate the values of principal stresses at a general interior point
- can require expensive equipment for precise analysis of large components
- is very tedious and time-consuming for three-dimensional work

Procedure

The procedure for preparing two-dimensional models from pre-machined templates will be described. Alternatively, specimens may be machined "from scratch," in which case a computer-controlled milling machine is recommended.

1. **Selecting the material.** Many polymers exhibit sufficient birefringence to be used as photoelastic specimen material. However, such common polymers as polymethylmethacrylate (PMMA) and polycarbonate may be either too brittle or too intolerant of localized straining. Homalite®-100 has long been a popular general-purpose material,[1] available in various thicknesses in large sheets of optical quality. PSM-1® is a more recently introduced material[2] that has excellent qualities, both for machining and for fringe sensitivity. Another good material is epoxy, which may be cast between plates of glass, but this procedure is seldom followed for two-dimensional work.
2. **Making a template.** If more than 2 or 3 pieces of the same shape are to be made, it is advisable to machine a *template* out of metal first. This template may then be used to fabricate multiple photoelastic specimens having the same shape as that of the template. The template should be undercut by about 0.050 in. through about half the template thickness from one side to avoid contact with the router bit (explained below).
3. **Machining the specimen.** If the specimen is machined "from scratch," care must be taken to

[1]Manufactured by Homalite Corporation, Wilmington, Del.

[2]Marketed by Measurements Group, Raleigh, N.C.

take very light cuts with a sharp milling cutter in order to avoid heating the specimen unduly along its finished edges. A coolant, such as ethyl alcohol, kerosene, or water, should be used to minimize heating.

If a template is used, then a bandsaw with a sharp, narrow bandsaw blade is used to rough out the shape of the specimen. A generous allowance of about 1/8 in. should be marked on the specimen all around the template edge, since the blade will heat the material and nick the edge. Then a router with a high-speed carbide router bit, preferably with fine multiple flutes, should be used to fabricate the edge of the model (Fig. 1). A succession of two centering pins—the first having a diameter larger than that of the router bit (as shown in the figure), and the second one the same size—should be used so that excess material can first be removed quickly, and then in a very controlled manner, leaving the specimen with the same dimensions as those of the template.

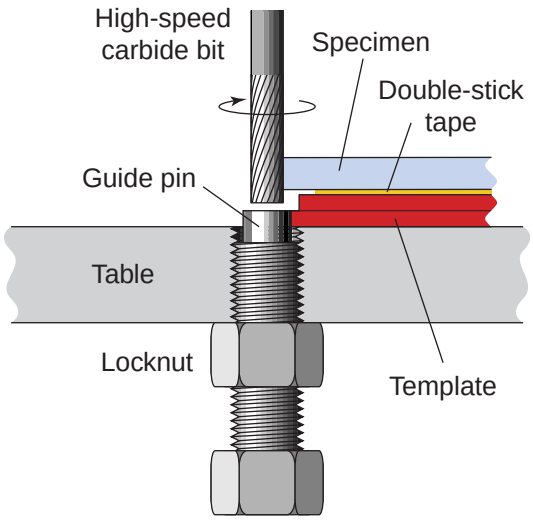

Fig. 1. Use of a template, router, and guide pin to rout the edge of a specimen.

The piece should always be forced *into* the cutting edge of the bit, that is, from front to back if the piece is on the right side of the bit (as in the figure). The final router passes should be smooth and very light so as to avoid heating of the specimen edges.

4. **Drilling the specimen.** If the specimen has holes, such as those used for load-application

points using pins, then these holes should be drilled carefully with a sharp bit with plenty of coolant, such as ethyl alcohol, kerosene, or water; otherwise unwanted fringes will develop around the edge of the hole. As illustrated in Fig. 2, the specimen should be backed with a sacrificial piece of similar material in order to avoid chipping on the back side of the specimen as the drill breaks through.

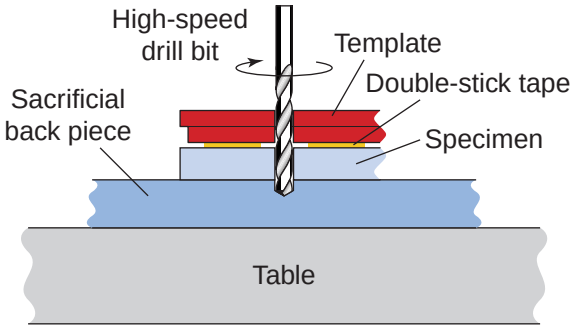

Fig. 2. Drilling a hole in the specimen.

A series of 2 or 3 passes of the drill bit through the specimen, with coolant added each time, will minimize heat-induced fringes.

5. **Viewing the loaded specimen.** After the specimen is removed from the template and cleaned, it is ready for loading. A polariscope (to be described later) is needed for viewing the fringes induced by the stresses. The elements of the polariscope must be arranged so as to allow light to propagate normal to the plane of the specimen. If a loading frame is needed to place a load on the specimen, then this frame must be placed between the first element(s) and the last element(s) of the polariscope. Monochromatic light should be used for the sharpest fringes; however, the light source does not need to be coherent, and the light may or may not be collimated as it passes through the specimen.

6. **Recording the fringe patterns.** An ordinary still camera or a videocamera may used to record the fringe patterns.

7. **Calibrating the material.** The sensitivity of a photoelastic material is characterized by its *fringe constant* f_σ, which relates the value N associated with a given fringe to the thickness h of the specimen in the light-propagation

direction and the difference between the principal stresses $\sigma_1 - \sigma_2$ in the plane normal to the light-propagation direction:

$$\sigma_1 - \sigma_2 = \frac{N f_\sigma}{h}.$$

By means of an experiment using a model of simple geometry subjected to known loading, the value of f_σ is determined. The disk in diametral compression is a common calibration specimen.

8. **Interpreting the fringe patterns.** Two types of pattern can be obtained: isochromatics and isoclinics. These patterns are related to the principal-stress differences and to the principal-stress directions, respectively. Details are given later in the notes below.

Wave theory of light

The theory of photoelasticity is based on the wave nature of light. Light is regarded as a sinusoidal electromagnetic wave having transverse amplitude *a* and longitudinal wavelength λ, propagating in the *z* direction with velocity *v* (Fig. 3).

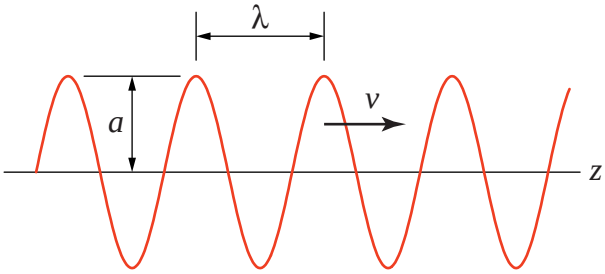

Fig. 3. Light wave.

A wave propagating in the +*z* direction may be represented in trigonometric notation as

$$a\cos\Phi = a\cos\left(\frac{2\pi}{\lambda}(z - vt)\right),$$

where the quantity $\Phi = \frac{2\pi}{\lambda}(z - vt)$ is called the *phase* of the wave. Terms related to the wavelength and speed are the ordinary frequency *f* (in Hz), the angular frequency ω (in rad/s), and the wave number *k*, as follows:

$$k = \frac{2\pi}{\lambda}, \qquad \omega = 2\pi\frac{v}{\lambda}, \qquad f = \frac{v}{\lambda}. \qquad (1)$$

Thus the phase has the alternative representations

$$\Phi = \frac{2\pi}{\lambda}(z - vt) = kz - \omega t = kz - 2\pi ft .$$

The speed of light v in a vacuum is approximately 299.79 Mm/s, independent of its wavelength or amplitude. From the last of the expressions in Eqns. (1), it will be seen that the frequency of a given light wave must depend on its wavelength:

Color	Speed, v (Mm/s)	Wavelength, λ (nm)	Frequency, f (THz)
Deep violet	299.79	400	750
Green	299.79	550	550
Deep red	299.79	700	430

Notice that the visible spectrum covers a nearly 2-to-1 ratio of wavelengths, the blue–violet wavelengths being much shorter than the orange–red ones.

An equivalent way to express the trigonometric form of a wave is in complex notation as

$$\mathrm{Re}\left\{ae^{i\Phi}\right\} = \mathrm{Re}\left\{ae^{i\frac{2\pi}{\lambda}(z-vt)}\right\} = \mathrm{Re}\left\{ae^{i(kz-\omega t)}\right\}.$$

Since the complex notation is much easier to manipulate when phases and amplitudes undergo changes, we shall use it in these notes. The operator Re{ } will be omitted for convenience, with the understanding that, if at any time a quantity is to be evaluated explicitly, the real part of the expression will be taken. A typical expression for a light wave will therefore be simply

$$A = ae^{i\Phi} = ae^{i\frac{2\pi}{\lambda}(z-vt)} = ae^{i(kz-\omega t)} . \qquad (2)$$

Refraction

When light passes through any medium, its velocity *decreases* to a value

$$v_1 = \frac{v}{n_1}, \qquad (3)$$

where n_1 denotes the *index of refraction* of the medium (Fig. 4). However, the frequency f of the

wave is unaffected. Therefore the wavelength λ_1 must also decrease proportionally:

$$\lambda_1 = \frac{v_1}{f} = \frac{v}{n_1 f} = \frac{\lambda}{n_1}.$$

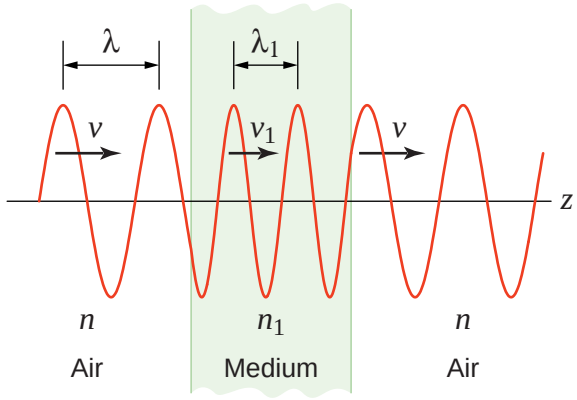

Fig. 4. Refraction.

Note that the time t_1 required for light to propagate through a thickness h of medium 1 having index of refraction n_1 is

$$t_1 = \frac{h}{v_1} = n_1 \frac{h}{v}.$$

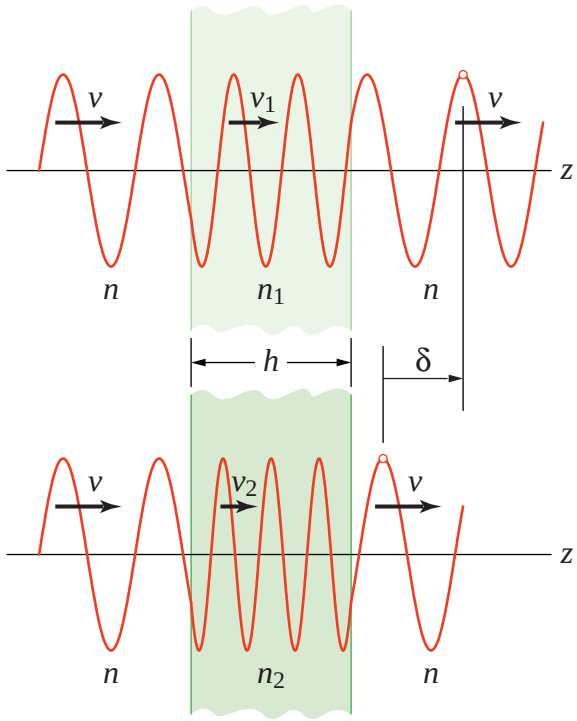

Fig. 5. Double refraction.

If similar light waves pass through the same thickness h of two media having indices of

refraction n_1 and n_2 (Fig. 5), and if $n_2 > n_1$ (as illustrated in the figure), then the difference in transit times $t_2 - t_1$ will be

$$t_2 - t_1 = \frac{h}{v_2} - \frac{h}{v_1} = \frac{h}{v}(n_2 - n_1).$$

Therefore, the phase difference δ between the two waves after they emerge from the media will be

$$\delta = v(t_2 - t_1) = h(n_2 - n_1). \qquad (3)$$

We will need this relation later when we consider birefringence of materials.

Polarization

A given light wave has an amplitude vector that is always *perpendicular* to its propagation direction. However, for ordinary light, the orientation of the amplitude vector in the plane perpendicular to the propagation direction is totally *random*.

Plane-polarized light

If the amplitude vectors of all light rays emanating from a source are restricted to a single plane, as in Fig. 6, the light is said to be *plane polarized*.

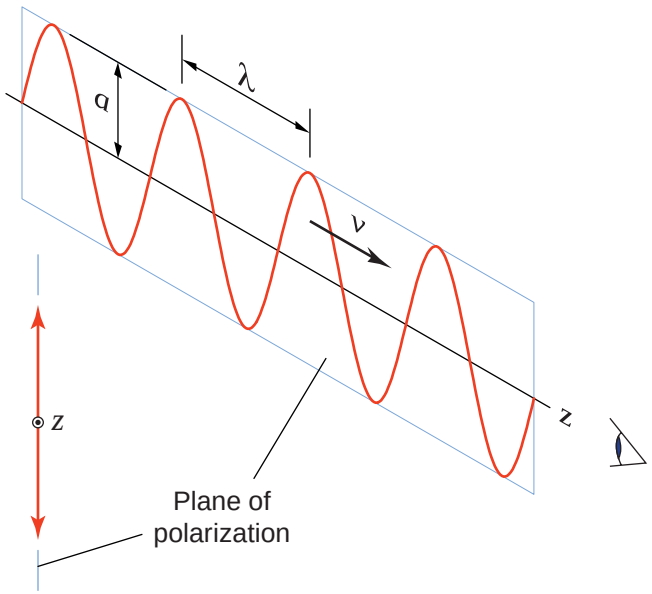

Fig. 6. Plane-polarized light.

An observer viewing the light wave head-on would see the wave with its amplitude vector restricted to a single plane, which is called the *plane of polarization*. This plane is not necessarily

vertical, as shown in the figure, but vertical polarization is quite common. Polaroid® sunglasses, for example, employ vertically polarizing media in both lenses to block the horizontally polarized light that is reflected from such horizontal surfaces as highways and lakes.

Addition of two plane-polarized waves in phase

If two waves are propagating in the same direction, vector algebra may be applied to the wave amplitudes to determine the resultant wave amplitude. Consider first the addition of two plane-polarized waves that are in phase, but that have different planes of polarization (Fig. 7).

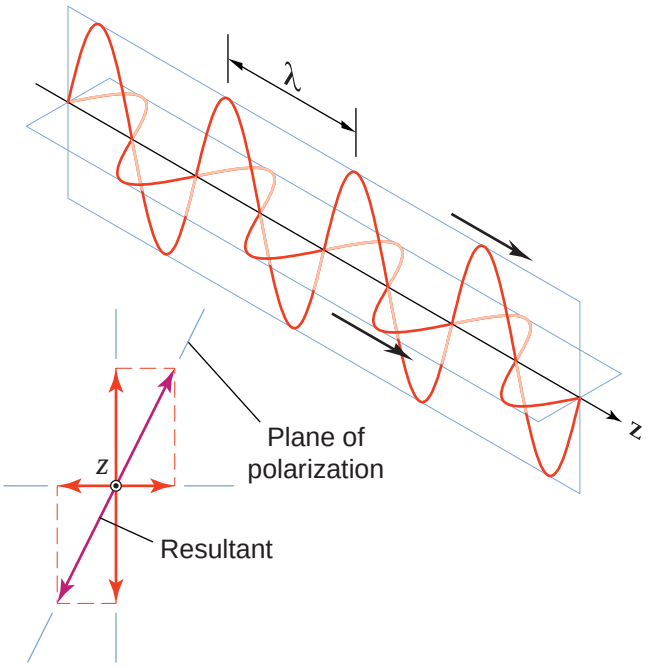

Fig. 7. Addition of two plane-polarized light waves that are in phase.

The vector addition of these two waves produces a new plane-polarized wave having the same frequency, wavelength, and phase as the component waves. Note that the two planes of polarization need not be orthogonal in order for this result to hold.

Elliptically polarized light

A more interesting case arises when two plane-polarized waves of arbitrary amplitude and different phase are combined (Fig. 8).

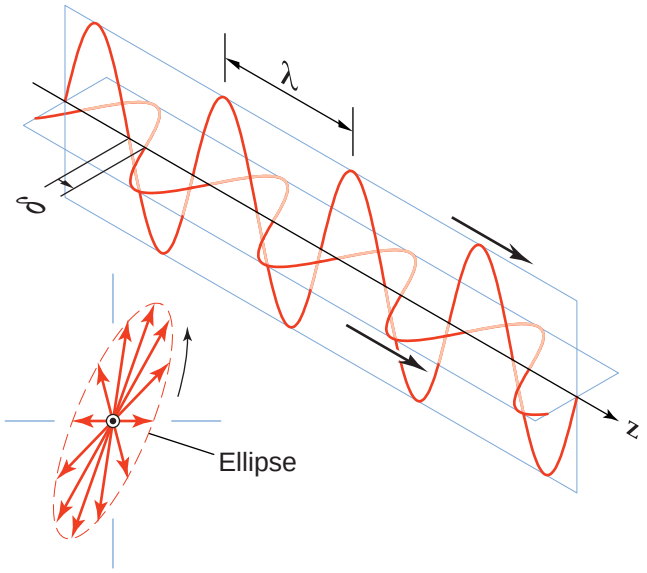

Fig. 8. Elliptically polarized light.

In the figure, the horizontally polarized wave is ahead of the vertically polarized wave by a distance δ, if we regard the positive senses for the horizontally and vertically polarized waves as being to the right and upward, respectively. At the instant shown, at the leading edge of the wave, the horizontal component is negative and the vertical component vanishes; therefore the resultant is in the negative horizontal direction. A tiny instant later, the horizontal component becomes slightly more negative and the vertical component rapidly becomes negative; therefore the resultant is in the fourth quadrant as viewed backwards along the +z axis. With increasing time, an elliptical path is traced by the amplitude vector of the resultant wave, as shown.

Thus the result of adding two plane-polarized waves that are neither in phase nor in the same plane is a special kind of rotating wave, called an *elliptically polarized wave*, having the same frequency as the component waves, but which is *not* restricted to a single plane.

Circularly polarized light

A very important special case of elliptically polarized light is *circularly polarized light*, which can be (and usually is) created by combining *orthogonal* plane-polarized waves of *equal* amplitude that are out of phase by *exactly* one-quarter of a wavelength, i.e. $\delta = \lambda / 4$. See Fig. 9.

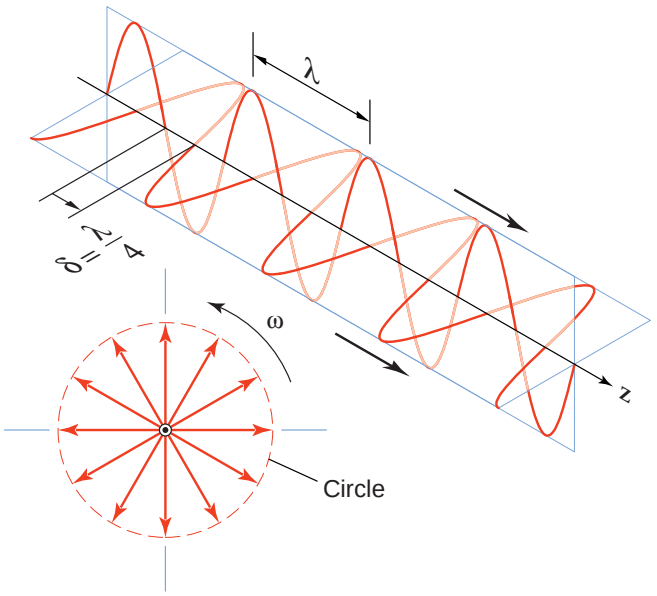

Fig. 9. Circularly polarized light.

For this special combination of plane waves, the resultant wave is a rotating wave having constant amplitude and constant angular frequency ω.

Optical elements

The method of photoelasticity requires the use of two types of optical element—the *polarizer* and the *wave plate*.

Polarizer

A polarizer (Fig. 10) is an element that converts randomly polarized light into plane-polarized light. It was the introduction of large polarizing sheets by Polaroid Corporation in 1934 that led to the rapid advance of photoelasticity as a stress-analysis tool. Prior to that, small naturally occurring crystals were used for this purpose.

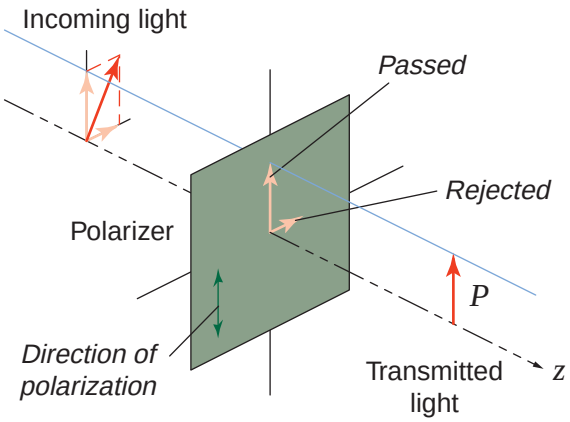

Fig. 10. Polarizer.

In the figure, a single light wave with arbitrarily oriented wave amplitude approaches the polarizer from the left. As this wave encounters the polarizer, it is resolved into two vector components—one parallel to the polarizing direction of the polarizer, and one perpendicular to it. The parallel component is passed, but the perpendicular one is *rejected*. Light emanating from the polarizer is therefore plane-polarized in the direction of polarization of the polarizer.

Viewed in ordinary (unpolarized) light, a polarizer always looks dark because half the light striking it is rejected.

Wave plate

A wave plate (Fig. 11) resolves incident light into two components, but instead of rejecting one of these components, it retards it relative to the other component.

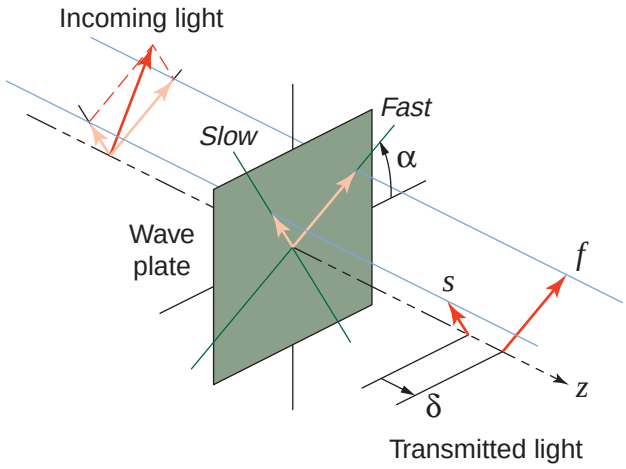

Fig. 11. Wave plate.

In the figure, the "fast" axis of the wave plate makes an angle α with respect to an arbitrarily chosen reference direction. The component *f* of the incident light with amplitude vector in this orientation is retarded somewhat as it passes through the wave plate. However, the orthogonal component *s* is retarded even more, resulting in a phase lag δ between this "slow" component and the "fast" one. The term *double refraction* is often used to describe this behavior.

Wave plates may be either permanent or temporary. A *permanent* wave plate has a fixed fast-axis orientation α and a fixed relative retarda-

tion δ. Such wave plates have their use in photoelasticity, as will be seen subsequently. A *temporary* wave plate has the ability to produce double refraction in response to mechanical stimulus. Photoelastic specimens are temporary wave plates.

Quarter-wave plate

A quarter-wave plate (Fig. 12) is a permanent wave plate that induces a phase shift δ equal to $\lambda / 4$, where λ is the wavelength of the light being used. The quarter-wave plate is an essential element in a circular polariscope (discussed later).

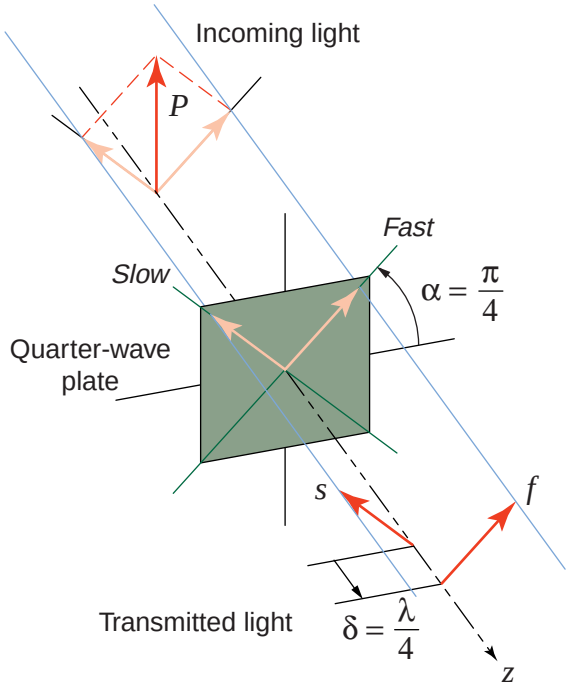

Fig. 12. Quarter-wave plate.

In Fig. 12, the incident light is assumed to have its amplitude vector in a vertical plane, and the fast axis of the quarter-wave plate has been oriented at 45° with respect to the horizontal axis. These special conditions have no bearing on the definition of a quarter-wave plate, but are often employed with a quarter-wave plate to produce circularly polarized light (Fig. 9)—observe that the orthogonal *f* and *s* components emanating under these special conditions have equal amplitude and are separated by exactly one-quarter wavelength.

The phase shift δ induced by any permanent wave plate is usually independent of the wavelength λ. Therefore, if a wave plate has been

designed to be a quarter-wave plate for green light (say $\lambda = 550$ nm), it will induce a relative phase shift δ equal to (550 nm)/4 or 138 nm. This same wave plate, if used for red light (say $\lambda = 650$ nm), will still induce an absolute phase shift of 138 nm, which is now only 138/650, or about 0.212, of the wavelength λ of red light. Quarter-wave plates are therefore said to be *imperfect*, not because of any manufacturing defect, but because the retardation expressed as a fraction of the wavelength is wavelength dependent.

Birefringence

Photoelastic materials are *birefringent*, that is, they act as temporary wave plates, refracting light differently for different light-amplitude orientations, depending upon the state of stress in the material.

In the unloaded state, the material exhibits an index of refraction n_0 that is independent of orientation. Therefore, light of all orientations propagating along all axes through the material propagate with the same speed, namely v / n_0.

In the loaded state, however, the orientation of a given light amplitude vector with respect to the principal stress axes, and the magnitudes of the principal stresses, determine the index of refraction for that light wave.

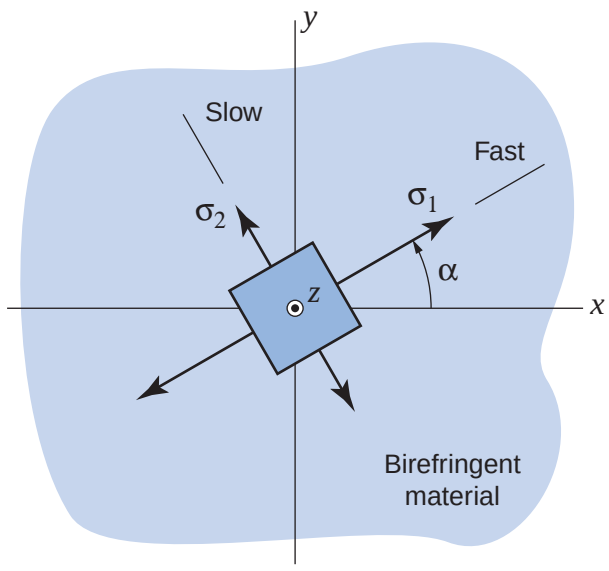

Fig. 13. Principal-stress element.

Effectively, a birefringent material acts as a temporary wave plate (Fig. 13). The index of refraction n_1 for light having its *amplitude vector* in the direction of the maximum principal normal stress σ_1 is given by

$$n_1 - n_0 = c_1\sigma_1 + c_2(\sigma_2 + \sigma_3), \qquad (4a)$$

where c_1 and c_2 are called the *stress-optic coefficients*, and, if birefringence is to occur, $c_1 \neq c_2$.

In a similar way, the index of refraction n_2 for light having its amplitude vector in the direction of the minimum principal normal stress σ_2 is given by

$$n_2 - n_0 = c_1\sigma_2 + c_2(\sigma_3 + \sigma_1), \qquad (4b)$$

and for light having its amplitude vector in the out-of-plane direction,

$$n_3 - n_0 = c_1\sigma_3 + c_2(\sigma_1 + \sigma_2). \qquad (4c)$$

Equations (4) are called Maxwell's equations.

Here, the light waves of interest are those propagating in the z direction, or σ_3 direction. These waves necessarily have their amplitude vectors in the xy plane, and we will therefore be interested mainly in Eqns. (4a) and (4b). It is always possible to resolve a given light amplitude vector into components aligned with the σ_1 and σ_2 axes. Let us suppose that light waves with amplitude vector in the σ_2 direction propagate more slowly through the material than those with amplitude vector in the σ_1 direction. Then $n_2 > n_1$. Now consider the emerging phase difference δ between orthogonal components M_1 and M_2 of a light wave that entered the material from the back in phase and that were aligned in the principal stress directions (Fig. 14). From Eqns. (4a,b),

$$\begin{aligned} n_2 - n_1 &= (c_2 - c_1)(\sigma_1 - \sigma_2) \\ &= c(\sigma_1 - \sigma_2), \end{aligned} \qquad (5)$$

where c is called the *relative stress-optic coefficient*, which is a material property. It is important to see in Eqn. (5) that the refraction-index difference $n_2 - n_1$ is *independent* of σ_3. The results to follow therefore hold for *arbitrary* value of σ_3; it is not necessary to assume that the material is in a state of plane stress.

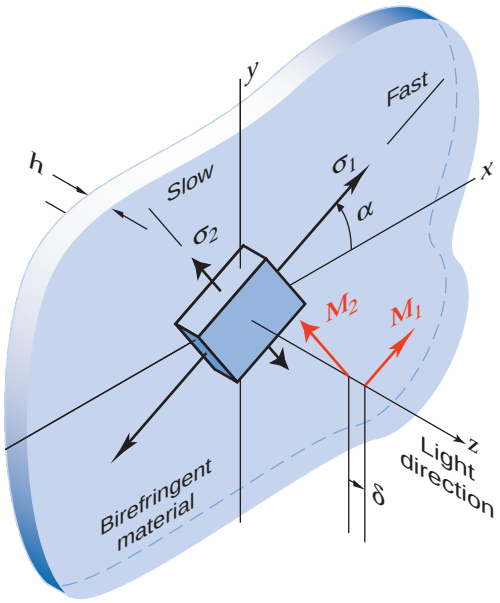

Fig. 14. Birefringent effect.

From Eqn. (5), and from Eqn. (3) derived earlier, we see that the phase difference δ between M_1 and M_2 is given by

$$\begin{aligned} \delta &= h(n_2 - n_1) \\ &= hc(\sigma_1 - \sigma_2), \end{aligned} \tag{6}$$

where h is the thickness of the material in the light-propagation direction (Fig. 14). This equation is of fundamental importance in the theory of photoelasticity. It is often written in terms of the number N of complete cycles of relative retardation, or, equivalently, in terms of the *angular phase difference* Δ, as follows:

$$N = \frac{\Delta}{2\pi} = \frac{\delta}{\lambda} = \frac{hc(\sigma_1 - \sigma_2)}{\lambda} = h\frac{\sigma_1 - \sigma_2}{f_\sigma}, \tag{7}$$

where f_σ is called the *fringe "constant"* of the material. The relative stress-optic coefficient c is found to be rather insensitive to the wavelength of the light. Therefore, the fringe "constant"

$$f_\sigma = \frac{\lambda}{c} \tag{8}$$

is anything but constant if light composed of many colors is used.

In summary, a birefringent material does two things:

- It resolves the incoming light into 2 components—one parallel to σ_1 and the other parallel to σ_2, and
- It retards one of the components, M_2, with respect to the other, M_1, by an amount δ that is proportional to the principal stress difference $\sigma_1 - \sigma_2$.

Polariscopes

A polariscope is an optical setup that allows the birefringence in specimens to be analyzed. It consists of a light source, a polarizer, an optional quarter-wave plate, a specimen, another optional quarter-wave plate, and a second polarizer called the *analyzer*. Two types of polariscope are commonly employed—the plane polariscope and the circular polariscope.

The plane polariscope

The plane polariscope (Fig. 15) consists of a light source, a polarizer, the specimen, and an analyzer that is *always* crossed with respect to the polarizer.

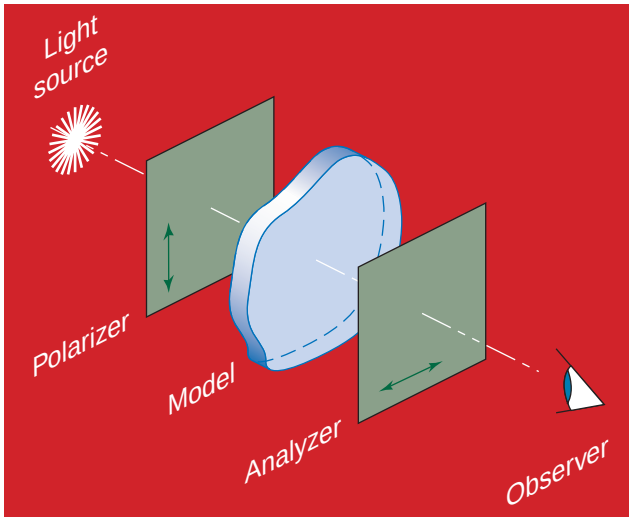

Fig. 15. The plane polariscope.

The direction of polarization of the polarizer is assumed to be vertical in the figure. We shall see later that it may be useful to rotate the polarizer and analyzer *together* in order to determine principal-stress directions, but in the derivation of the polariscope equations, there is no loss of generality by assuming that the light leaving the polarizer (Fig. 16) is vertically polarized.

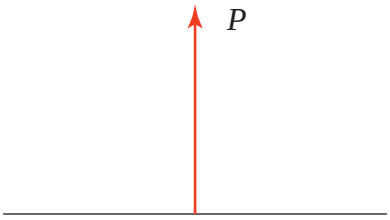

Fig. 16. Light leaving polarizer.

Let P designate the light leaving the polarizer. The orientation of P is vertical; its amplitude is a, and its phase Φ is that of a traveling wave, namely,

$$\Phi = \frac{2\pi}{\lambda}(z - ct) = kz - \omega t\,.$$

Therefore, its complex representation is

$$P = ae^{i\Phi}\,. \tag{9}$$

Now consider the light leaving the specimen (Fig. 17).

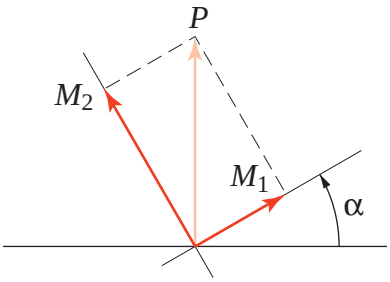

Fig. 17. Light leaving model (plane polariscope).

This light has been resolved into a fast component M_1 having amplitude

$$M_1 = P\sin\alpha \tag{10a}$$

and a retarded component M_2 having amplitude $P\cos\alpha$. However, this retarded component is not in phase with the fast component; it lags the fast component by an angular phase shift

$$\Delta = k\delta = 2\pi\frac{\delta}{\lambda}\,.$$

Therefore its correct complex representation is

$$M_2 = Pe^{i\Delta}\cos\alpha\,. \tag{10b}$$

The correct sign of the angular phase shift can be checked by examining two waves propagating in the $+z$ direction (Fig. 18). The blue wave is lagging the red wave by the amount δ as both waves propagate

to the right. If, at time $t = 0$, the red wave has the representation $\cos[kz]$, then the blue wave has the representation $\cos[k(z+\delta)]$.

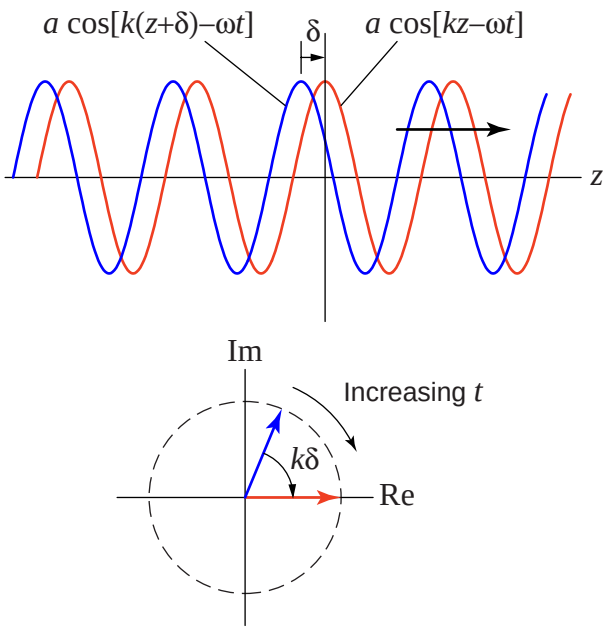

Fig. 18. Phase shift at time $t = 0$.

The Argand diagram in the figure illustrates perhaps more clearly the relations between z, δ, and time t. With increasing time, the vectors representing the amplitude and phase of the slow and fast waves rotate clockwise. The projections of the amplitudes on the real axis give the actual amplitudes at any instant t and position z. The red wave is clearly ahead of the blue wave if the retardation $\Delta = k\delta$ is taken in the positive sense as indicated.

Finally, we consider the light leaving the analyzer (Fig. 19). In a plane polariscope, the analyzer is *always* crossed with respect to the polarizer. Since the polarizer was assumed to be vertically oriented, the analyzer is horizontally oriented.

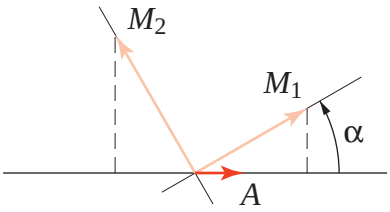

Fig. 19. Light leaving analyzer (plane polariscope).

The analyzer rejects all vertically polarized components of light and passes the horizontally polarized components, so that

$$\begin{aligned} A &= M_1 \cos\alpha - M_2 \sin\alpha \\ &= (P\sin\alpha)\cos\alpha - (Pe^{i\Delta}\cos\alpha)\sin\alpha \\ &= P\sin\alpha\cos\alpha\left(1-e^{i\Delta}\right). \end{aligned}$$

We note that

$$\sin\alpha\cos\alpha = \tfrac{1}{2}\sin 2\alpha$$

and that

$$\begin{aligned} 1-e^{i\Delta} &= e^{i\Delta/2}\left(e^{-i\Delta/2}-e^{i\Delta/2}\right) \\ &= e^{i\Delta/2}\left(-2i\sin\frac{\Delta}{2}\right). \end{aligned}$$

Therefore, by making use of the original representation of P, Eqn. (9), the expression for A simplifies to

$$\begin{aligned} A &= -ie^{i\Delta/2}ae^{i\Phi}\sin 2\alpha\sin\frac{\Delta}{2} \\ &= ae^{i(-\pi/2+\Delta/2+\Phi)}\sin 2\alpha\sin\frac{\Delta}{2}. \end{aligned}$$

In this expression, as in many like it to follow, it is important to realize that a factor like $e^{i(-\pi/2+\Delta/2+\Phi)}$ has a magnitude equal to unity. Therefore, the magnitude of A is simply

$$|A| = a\sin 2\alpha\sin\frac{\Delta}{2}.$$

The *intensity* of light I leaving the analyzer is given by the square of the light amplitude. Thus, for the plane polariscope, the intensity of the light seen by the observer is

$$I = |A|^2 = a^2\sin^2 2\alpha\sin^2\frac{\Delta}{2}. \qquad (11)$$

Isoclinics and isochromatics

The human eye is very sensitive to minima in light intensity. From Eqn. (11), it is seen that *either one* of two conditions will prevent light that passes through a given point in the specimen from reaching the observer, when a plane polariscope is used.

The first condition is that

$$\sin^2 2\alpha = 0, \quad \text{i.e.}$$
$$\alpha = m\frac{\pi}{2}, \quad m = 0, \pm 1, \pm 2, \cdots. \tag{12}$$

Since α is the angle that the maximum principal normal stress makes with the polarizing direction of the analyzer, this result indicates that all regions of the specimen where the principal-stress directions are aligned with those of the polarizer and analyzer will be dark. The locus of such points is called an *isoclinic* because the orientation, or inclination, of the maximum principal normal stress direction is the same for all points on this locus. By rotating *both* the analyzer and polarizer together (so that they stay mutually crossed), isoclinics of various principal-stress orientations can be mapped throughout the plane. Several examples are given in the text (Dally and Riley 1991).

The second condition is that

$$\sin^2 \frac{\Delta}{2} = 0, \quad \text{i.e.}$$
$$N = \frac{\Delta}{2\pi} = n, \quad n = 0, 1, 2, \cdots. \tag{13}$$

The locus of points for which this condition is met is called an *isochromatic*, because (except for $n = 0$) it is both stress *and* wavelength dependent. Recall from Eqn. (7) that

$$N = \frac{\Delta}{2\pi} = \frac{\delta}{\lambda} = \frac{hc(\sigma_1 - \sigma_2)}{\lambda} = h\frac{\sigma_1 - \sigma_2}{f_\sigma}.$$

Therefore, points along an isochromatic in a plane polariscope satisfy the condition

$$\sigma_1 - \sigma_2 = N\frac{\lambda}{ch} = \frac{Nf_\sigma}{h}, \quad N = n. \tag{14}$$

The number n is called the *order* of the isochromatic. If monochromatic light is used, then the value of λ is unique, and very crisp isochromatics of very high order can often be photographed. (Examples will be given later.) However, if white light is used, then (except for $n = 0$), the locus of points for which the intensity vanishes is a function of wavelength. For example, the locus of points for which red light is extinguished is generally not a locus for which green or blue light is extinguished, and therefore some combination of blue and green will be transmitted wherever red is not. The result is a

very colorful pattern, to be demonstrated by numerous examples in class using a fluorescent light source.[3]

The circular polariscope—dark field

The circular polariscope (Fig. 20) consists of a light source, a polarizer, a quarter-wave plate oriented at 45° with respect to the polarizer, the specimen, a second quarter-wave plate, and an analyzer.

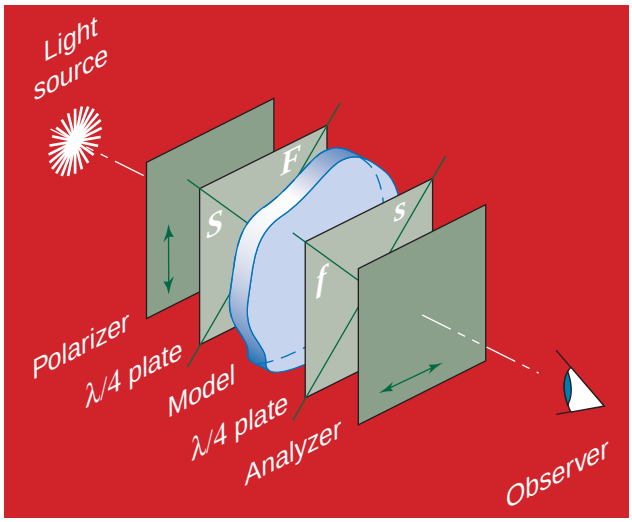

Fig. 20. Circular polariscope (dark field).

The two quarter-wave plates are generally crossed (as shown in the figure) to minimize error due to imperfect quarter-wave plates. The analyzer is either crossed with respect to the polarizer (as shown in the figure), or parallel to the polarizer.

Again, the direction of polarization of the polarizer is assumed to be vertical (Fig. 16), and we take as a representation of the polarized light leaving the polarizer the expression (Eqn. (9))

$$P = ae^{i\Phi} .$$

This light enters the first quarter-wave plate and leaves with the two components

[3]However, this interference of colors results in a "washing out" of the higher-order isochromatics and is particularly troublesome if a panchromatic black-and-white film is used to record the isochromatic patterns. A way to minimize the loss of data due to washing out is to photograph the isochromatic patterns with color film and to scan the color negative digitally, separating out the red, green, and blue components. The component with the sharpest fringes can then be used for analysis.

$$
\begin{aligned}
F &= \frac{P}{\sqrt{2}}, \\
S &= \frac{P}{\sqrt{2}} e^{i\pi/2} \\
&= i\frac{P}{\sqrt{2}},
\end{aligned}
\tag{15}
$$

as illustrated in Fig. 21. Comparison of this figure with Fig. 9 shows that this arrangement produces circularly polarized light that is rotating counter-clockwise.

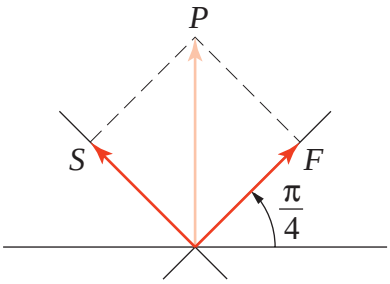

Fig. 21. Light leaving first quarter-wave plate (circular polariscope).

Light components leaving the specimen are shown in Fig. 22. The angle $\phi = \frac{\pi}{4} - \alpha$ that F makes with M_1 is introduced for convenience.

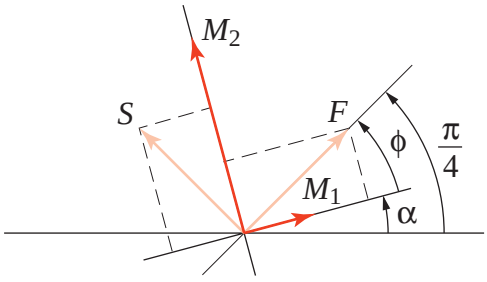

Fig. 22. Light leaving model (circular polariscope).

Taking into account the relative retardation Δ that the specimen introduces with respect to the principal stress planes, we have

$$
\begin{aligned}
M_1 &= F\cos\phi - S\sin\phi \\
&= \frac{P}{\sqrt{2}}(\cos\phi - i\sin\phi) \\
&= \frac{P}{\sqrt{2}}e^{-i\phi}\,, \\
M_2 &= (F\sin\phi + S\cos\phi)e^{i\Delta} \\
&= \frac{P}{\sqrt{2}}(\sin\phi + i\cos\phi)e^{i\Delta} \\
&= i\frac{P}{\sqrt{2}}(\cos\phi - i\sin\phi)e^{i\Delta} \\
&= i\frac{P}{\sqrt{2}}e^{i(\Delta-\phi)}\,.
\end{aligned}
\tag{16}
$$

Now consider the light leaving the second quarter-wave plate (Fig. 23). As mentioned earlier, the second quarter-wave plate is usually crossed with respect the first quarter-wave plate. Therefore, it has the effect of "derotating" the light that was "rotated" by the first quarter-wave plate.

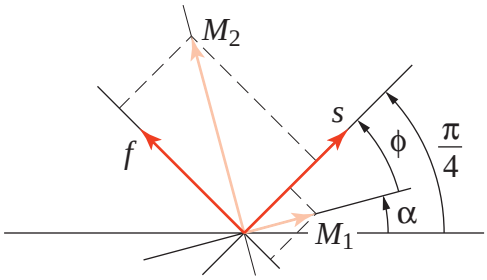

Fig. 23. Light leaving the second quarter-wave plate (circular polariscope).

Components s and f have the expressions

$$
\begin{aligned}
s &= (M_1\cos\phi + M_2\sin\phi)e^{i\pi/2} \\
&= \frac{P}{\sqrt{2}}e^{-i\phi}(\cos\phi + ie^{i\Delta}\sin\phi)i\,, \\
f &= -M_1\sin\phi + M_2\cos\phi \\
&= \frac{P}{\sqrt{2}}e^{-i\phi}(-\sin\phi + ie^{i\Delta}\cos\phi) \\
&= \frac{P}{\sqrt{2}}e^{-i\phi}(i\sin\phi + e^{i\Delta}\cos\phi)i\,.
\end{aligned}
\tag{17}
$$

Finally, if the analyzer is crossed with respect to the polarizer, as shown in Fig. 24, then its output A is given by the expression

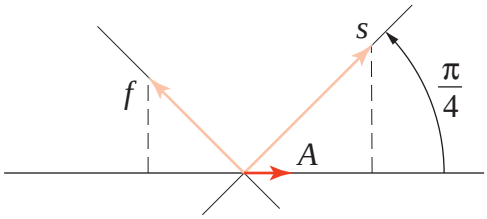

Fig. 24. Light leaving analyzer (circular polariscope).

$$\begin{aligned} A &= \frac{1}{\sqrt{2}}(s-f) \\ &= \frac{P}{2}e^{-i\phi}i\left(\cos\phi + ie^{i\Delta}\sin\phi - i\sin\phi - e^{i\Delta}\cos\phi\right) \\ &= \frac{P}{2}e^{-i\phi}i(\cos\phi - i\sin\phi)\left(1-e^{i\Delta}\right) \\ &= \frac{P}{2}e^{-i\phi}ie^{-i\phi}\left(1-e^{i\Delta}\right) \\ &= \frac{P}{2}e^{-i2\phi}ie^{i\Delta/2}\left(-2i\sin\frac{\Delta}{2}\right) \\ &= Pe^{-i2\phi}e^{i\Delta/2}\sin\frac{\Delta}{2}. \end{aligned}$$

Since $P = ae^{i\Phi}$ as before, the magnitude of A is just

$$|A| = a\sin\frac{\Delta}{2},$$

and the intensity I of the light leaving the analyzer is

$$I = |A|^2 = a^2\sin^2\frac{\Delta}{2}. \qquad (18)$$

This result is similar to that for the plane polariscope, with the notable absence of the factor $\sin^2 2\alpha$. Therefore, a circular polariscope produces isochromatics but not isoclinics. The lack of isoclinics is often desirable, since the dark isoclinics in a plane polariscope often obscure large areas of the model. For this reason, most of the photoelastic patterns published in the literature are obtained with a circular polariscope.

An examination of Eqn. (18) shows that, when there is no model, or when the model is unstressed, i.e. $\Delta = 0$ everywhere, the entire field is *dark*. The circular polariscope configuration just studied is therefore called the *dark field* configuration. The isochromatic pattern is analyzed in exactly the same manner as that for the plane polariscope, i.e.

$$\sigma_1 - \sigma_2 = N\frac{\lambda}{ch} = \frac{Nf_\sigma}{h}, \quad N = n. \qquad (19)$$

The circular polariscope—light field

An important simple variation on the arrangement of elements in a circular polariscope is one in which the quarter-wave plates remain crossed and the analyzer is aligned *parallel* to the polarizer (Fig. 25).

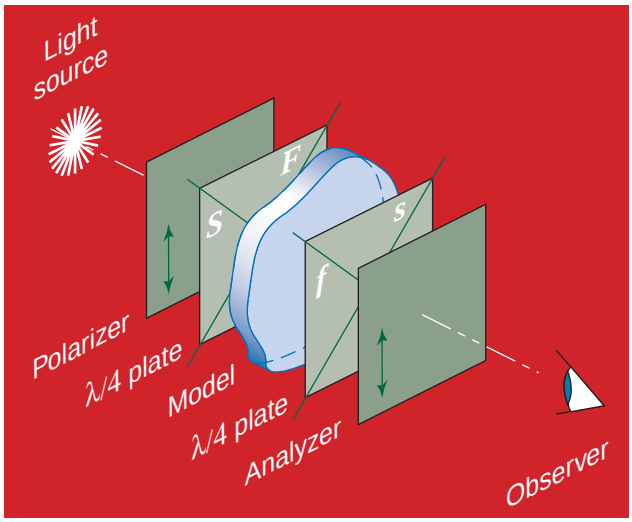

Fig. 25. Circular polariscope (light field).

In this case, the output A of the analyzer becomes

$$A = \frac{1}{\sqrt{2}}(s+f),$$

where s and f are the slow and fast components leaving the second quarter-wave plate (Eqns. (17)). One can show that the intensity of light leaving the analyzer is now given by

$$I = |A|^2 = a^2 \cos^2 \frac{\Delta}{2}. \qquad (20)$$

Therefore, in the absence of a model, or for a model that is unloaded, the intensity is at its maximum. This configuration is called the *light field* configuration. In many cases the light-field arrangement is preferred over the dark-field one because the boundary of the model is seen more clearly. The only difference in isochromatic interpretation is that the intensity now vanishes wherever $\cos^2 \frac{\Delta}{2} = 0$, i.e.

$$N = \frac{\Delta}{2\pi} = n + \tfrac{1}{2}, \quad n = 0, 1, 2, \cdots. \qquad (21)$$

The *dark* isochromatics in a light-field circular polariscope therefore correspond to the orders $\frac{1}{2}$, $1\frac{1}{2}$, $2\frac{1}{2}$, etc., instead of integer values, i.e.

$$\sigma_1 - \sigma_2 = N\frac{\lambda}{ch} = \frac{Nf_\sigma}{h}, \quad N = n + \tfrac{1}{2}. \quad (22)$$

The *light* isochromatics in a light-field circular polariscope correspond to the integer values of N. Since f_σ is wavelength dependent, the only isochromatic that is unaffected by the color content of the light source is the zero order one, which is *light*.

Calibration

The value of the fringe constant f_σ can be determined experimentally by inducing a known stress difference $\sigma_1 - \sigma_2$ in a model that is made of the same material as the specimen of interest, by observing the corresponding value of N, and by solving Eqn. (7) for f_σ:

$$f_\sigma = h\frac{\sigma_1 - \sigma_2}{N}. \quad (23)$$

Observe that strongly birefringent materials will have *low* values of f_σ, since the stresses required to produce a given value of N will be small.

A common calibration specimen is the circular disk of diameter D and thickness h loaded in diametral compression (Fig. 26).

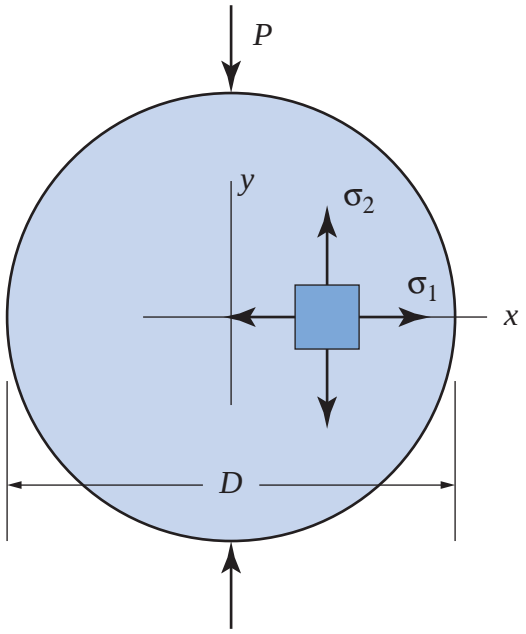

Fig. 26. Disk in compression.

The horizontal and vertical normal stresses along the x axis are principal stresses because the shear stress τ_{xy} vanishes due to symmetry about the x axis. Also, σ_x is positive, while σ_y is negative. We therefore take $\sigma_1 = \sigma_x$ and $\sigma_2 = \sigma_y$ so as to render $\sigma_1 - \sigma_2 \geq 0$. From theory of elasticity, the solutions for the normal stresses along the horizontal diameter are (after Dally and Riley 1991)

$$\begin{aligned} \sigma_1 &= \frac{2P}{\pi h D}\left(\frac{1-\zeta^2}{1+\zeta^2}\right)^2, \\ \sigma_2 &= -\frac{6P}{\pi h D}\frac{\left(1-\zeta^2\right)\left(1+\frac{1}{3}\zeta^2\right)}{\left(1+\zeta^2\right)^2}, \end{aligned} \tag{24}$$

where $\zeta = x/R = 2x/D$. These stresses are plotted in Fig. 27.

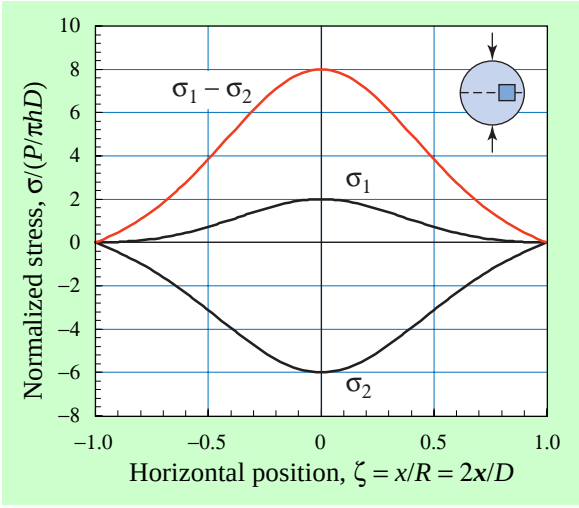

Fig. 27. Stress distribution along horizontal diameter.

Along the horizontal diameter, the maximum difference $\sigma_1 - \sigma_2$ occurs at the center, that is, at $\zeta = 0$. At this point,

$$\sigma_1 - \sigma_2 = \frac{8P}{\pi h D}. \tag{25}$$

Combining this result with the basic photoelastic relation (Eqn. (7)) gives

$$\frac{N f_\sigma}{h} = \sigma_1 - \sigma_2 = \frac{8P}{\pi h D},$$

or

$$f_\sigma = \frac{8}{\pi D}\frac{P}{N}. \tag{26}$$

Notice that the specimen thickness h does not appear in this equation. The reason is that the relative retardation is proportional to h, but for a given force P, the stresses are inversely proportional to h. The net effect is a result for f_σ that is independent of h. A photograph of a light-field isochromatic pattern for a diametrally loaded disk made of PSM-1® is shown in Fig. 28.

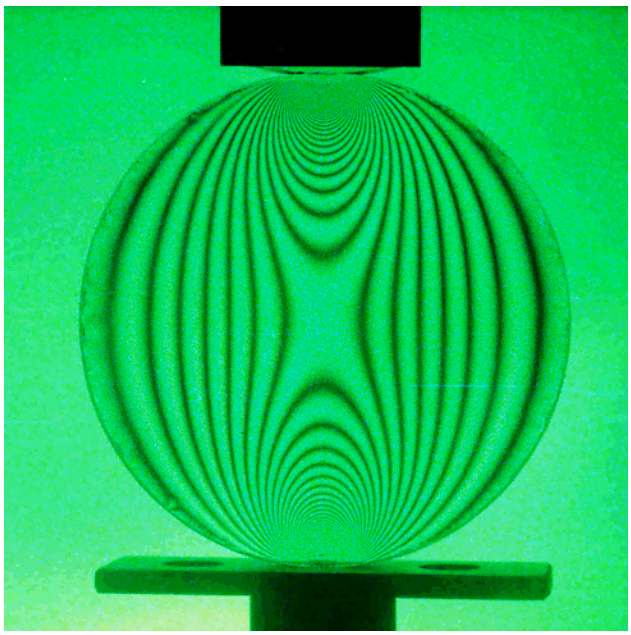

Fig. 28. Light-field isochromatics in a diametrally loaded circular disk.

For this specimen, the diameter D was 63.50 mm (2.500 in.), and the load was 1.33 kN (298 lb). The value of N at the center of the disk, as seen in Fig. 28, is approximately 7.0. Therefore the fringe constant for this material is approximately

$$f_\sigma = \frac{8}{\pi D}\frac{P}{N} = \frac{8}{\pi(2.500)}\frac{298}{7.0} = 43\,\frac{\text{psi}\cdot\text{in.}}{\text{fringe}}.$$

A more accurate way of determining f_σ using this specimen is to record several readings of increasing load P as the fringe value N at the center takes on integer or half-integer values. The saddle shape of the central fringe allows rather precise determination of N for this purpose. Then P is plotted as a function of N, and the best straight-line fit of the data is used to determine the ratio P / N to be used in Eqn. (26).

The disk in diametral compression is a favorite specimen for calibration because it is simple to fabricate (at least with a template); it is easy to load;

it is not likely to fracture; it produces a fringe pattern that, in the region of interest, is insensitive to edge imperfections; and it is simple to analyze. It also tests the limit of fringe density that can be recorded photographically, by producing very large fringe orders in the vicinity of the contact regions.

The image in Fig. 28 was obtained with a mercury-vapor light source, which is rich in green light, but which also contains other colors as well. A Tiffen #58 Green filter was placed on the 35 mm camera to reduce the transmission of the other colors. Kodak Gold ASA 200 color film was used to record the image at f/8 with an exposure of 0.7 s. This arrangement results in distinct fringes up to about $N = 15$, which is adequate for most work in photoelasticity.

A somewhat enhanced image is shown in Fig. 29. This image was produced from the same negative as that used to produce Fig. 28. However, only the green component of the red-green-blue (RGB) digital scan was retained, and this component was then enhanced by increasing the contrast.

Fig. 29. Enhanced image using only the green component of the light used in Fig. 28.

Fringe orders up to about $N = 20$ can be discerned in this figure. The low-order values of N are marked along the horizontal diameter. Note that the center of the specimen is the location of a true saddle point in the function $\sigma_1 - \sigma_2$: to the left and

right of this point, the function decreases, and above and below this point, the function increases. Such saddle points are common in photoelastic patterns, as will be seen in other examples to be given below.

The stress distribution in a disk in diametral compression is unique in that the fringe number N is equal to zero everywhere along the unloaded boundary.

Examples

Several photoelastic patterns will be presented for common structural shapes. These include the uniform beam in 4-point bending, as well as beams having cutouts; a compact-tension specimen; and a straight–curved "U" specimen.

A light-field circular polariscope with the recording and processing methods described in connection with Fig. 29 will be used.

Beam in bending

Consider first a uniform rectangular beam subjected to 4-point bending (Fig. 30).[4] Let x and y denote positions along the horizontal and vertical axes having their origin at the center of the specimen.

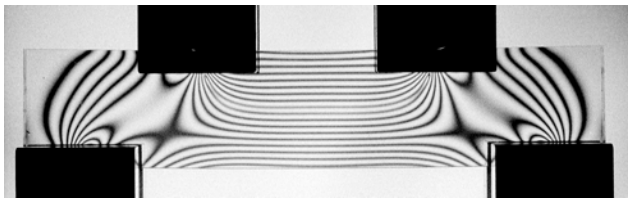

Fig. 30. Beam in 4-point bending.

Within the central portion of the beam, the bending moment is constant and, according to elementary beam theory, the axial stress σ_x is given by $-My / I$, varying from $-Mc / I$ at the top surface to Mc / I at the bottom surface. Also within this region, the transverse shear V vanishes, and therefore $\tau_{xy} = 0$ in this region. In addition, $\sigma_y = 0$.

[4]Specimen material, PSM-1. Load, 150 lb. Beam length, 5 in. Beam height, 1.000 in. Beam thickness, 0.213 in. Distance between lower supports, 4.00 in. Distance between upper supports, 2.00 in.

Since $\tau_{xy} = 0$, the normal stresses σ_x and σ_y are principal stresses. It follows that

$$\sigma_1 - \sigma_2 = \left|\sigma_x - \sigma_y\right| = \left|-\frac{My}{I} - 0\right| = \frac{M}{I}|y|,$$

with the understanding that *M* is positive.

We have to be careful about the signs of the principal stresses because we want $\sigma_1 - \sigma_2 \geq 0$. With this convention, the fringe number *N* will always be positive or zero. If one argues that negative values of *N* should be allowed (whether or not $\sigma_1 - \sigma_2 \geq 0$), one runs into inconsistencies. Consider, for example, the centrally located fringes in Fig. 30. There is a zero-order (light) fringe at the very center, along the neutral axis of bending. It is surrounded by a continuous dark fringe of order $N = \frac{1}{2}$. If we assigned a value of *N* equal to $-\frac{1}{2}$ on the top portion (where the axial stress is negative), and a value equal to $+\frac{1}{2}$ on the bottom portion (where the axial stress is positive), we would not be able to reconcile the value of *N* at the ends of the loop. It cannot vary along the loop because by definition the isochromatic is a locus of constant *N*.

Let us calculate the stress at the top and bottom of the beam. We know that f_σ is about 43 psi·in./fringe for this material, and by counting fringes in Fig. 30, we determine that *N* = 9 at both the top and bottom of the beam. To calculate $\sigma_1 - \sigma_2$, we also need to know the thickness *h*. For the specimen in Fig. 30, *h* = 5.41 mm (0.213 in.). Therefore, at the extreme fibers,

$$\left|\sigma_x\right| = \sigma_1 - \sigma_2 = \frac{Nf_\sigma}{h} = \frac{9(43)}{(0.213)} = 1.8 \text{ ksi}.$$

At the top, σ_x is negative, so it is equal to –1.8 ksi there; whereas, at the bottom, σ_x is positive, so it is equal to +1.8 ksi. This simple example serves to illustrate the point that photoelastic analysis requires *some* knowledge about the stress state in order to interpret the fringes correctly.

We can check these results. For the given beam, $M = \frac{1}{2}Pa$, $I = \frac{1}{12}hH^3$, $c = \frac{1}{2}H$, and therefore

$$|\sigma_x| = \frac{Mc}{I} = \frac{\left(\frac{1}{2}Pa\right)\left(\frac{1}{2}H\right)}{\frac{1}{12}hH^3} = \frac{3Pa}{hH^2}$$

$$= \frac{3(150)(1.00)}{(0.213)(1.000)^2} = 2.1\ \text{ksi}\,.$$

The predicted stresses are slightly higher than those observed, suggesting perhaps that friction at the supports may be reducing the effective value of *M*.

Beam with a keyhole notch

The stress distribution is altered drastically if a fillet, crack, or notch is machined into the specimen. The stress-concentration effect of a "keyhole" notch is shown in Fig. 31.[5]

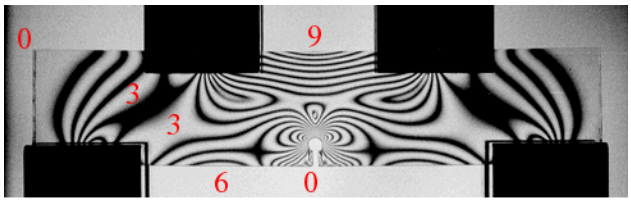

Fig. 31. Beam with keyhole notch.

The resolution of this image does not permit an exact determination of the stress-intensity factor for the notch, but it is clear that the stress at the root of the notch is much larger in tension than the compressive stress at the top of the beam, where the fringe number *N* happens to have the value 9 as it did in the previous uniform beam at a higher load. A reduced load and/or an improved imaging method would be needed to resolve the fringes at the root of the notch.

This specimen provides a good lesson in fringe counting. At all exterior corners, including the upper and lower corners on *each* side of the notch, $N = 0$. Also, $N = 0$ in the tiny triangular "island" just above the notch, and $N = 0$ in the "eyes" between the notch and each upper support. Remnants of the uniform bending field are seen between the upper supports.

There are 4 saddle points to the left of the centerline, and a matching set of 4 to the right. On the left, starting from the left, they have the approximate values $N = 3\frac{1}{2}$, 3, $4\frac{1}{2}$, and 2.

[5]Load, 100 lb. Other parameters are the same as for the uniform beam.

Beam with a sharp notch

An even sharper discontinuity is illustrated in Fig. 32.[6] Here, the notch was produced with a milling cutter having a 45° tip. The tip has a small radius; if the tip had been absolutely sharp, the specimen would probably have broken before this picture could have been taken.

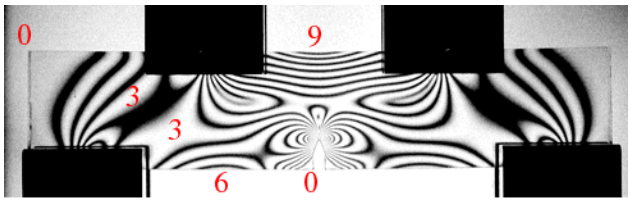

Fig. 32. Beam with sharp notch.

The stress field away from the sharp notch resembles very closely the stress field for the keyhole notch. The 4 saddle points seen earlier are evident in this photograph as well. Details of the stress field around the notch would require a smaller load on the beam and an improved method of recording the fringe patterns.

Compact-tension specimen

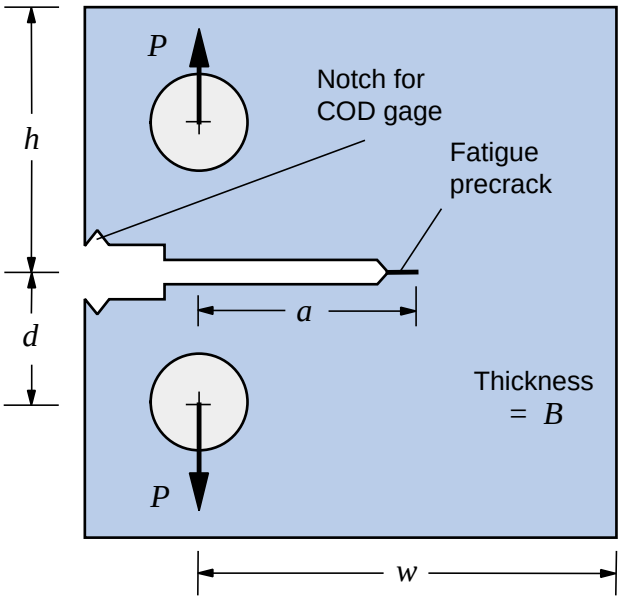

Fig. 33. Compact-tension specimen.

[6]Load, 100 lb. Other parameters are the same as for the uniform beam.

Perhaps the most common specimen used to determine experimentally the fracture toughness K_{IC} of materials is the compact-tension specimen (Fig. 33).

In the region of the crack tip, the stress field is dominated by the K_I singularity (Fig. 34).

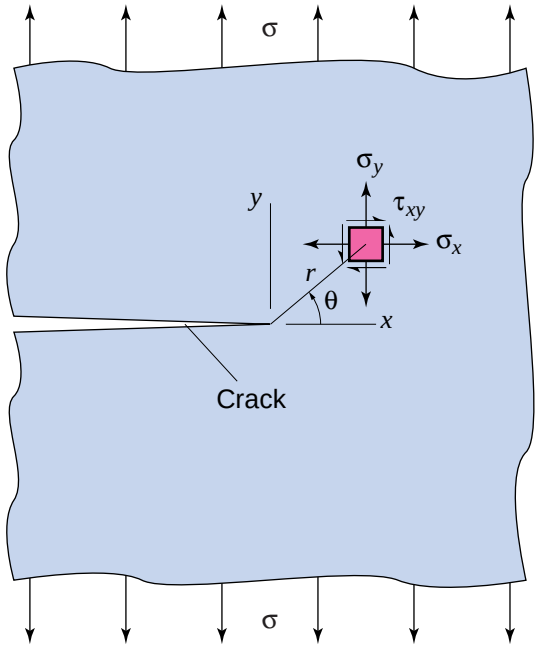

Fig. 34. Stress element near the crack tip in mode I loading.

Under plane strain or plane stress conditions, if the stresses remain elastic, the stress distribution can be shown to be

$$\begin{Bmatrix} \sigma_x \\ \sigma_y \\ \tau_{xy} \end{Bmatrix} = \frac{K_I}{\sqrt{2\pi r}} \cos\frac{\theta}{2} \begin{Bmatrix} 1-\sin\frac{\theta}{2}\sin\frac{3\theta}{2} \\ 1+\sin\frac{\theta}{2}\sin\frac{3\theta}{2} \\ \sin\frac{\theta}{2}\cos\frac{3\theta}{2} \end{Bmatrix}, \quad (27)$$

where K_I is the stress-intensity factor, which is a function of the specimen geometry and the remotely applied load. For this distribution, the in-plane principal-stress difference $\sigma_1 - \sigma_2$ can be calculated; the result is

$$\begin{aligned} \sigma_1 - \sigma_2 &= 2\sqrt{\left(\frac{\sigma_x - \sigma_y}{2}\right)^2 + \tau_{xy}^2} \\ &= \frac{K_I}{\sqrt{2\pi r}} |\sin\theta| . \end{aligned} \quad (28)$$

Combining this theoretical formula with the basic equation of photoelasticity gives

$$\frac{Nf_\sigma}{h} = \sigma_1 - \sigma_2 = \frac{K_I}{\sqrt{2\pi r}}|\sin\theta|$$

or

$$N(r,\theta) = \frac{h}{f_\sigma}\frac{K_I}{\sqrt{2\pi r}}|\sin\theta| . \qquad (29)$$

Alternatively, this equation may be solved parametrically for r in terms of θ:

$$r = \frac{1}{2\pi}\left(\frac{hK_I}{Nf_\sigma}\right)^2 \sin^2\theta .$$

This solution allows us to construct the theoretical photoelastic fringes, as shown in Fig. 35. These fringes look like nested ellipses, but the shapes are not really ellipses—they become almost pointed at the crack tip.

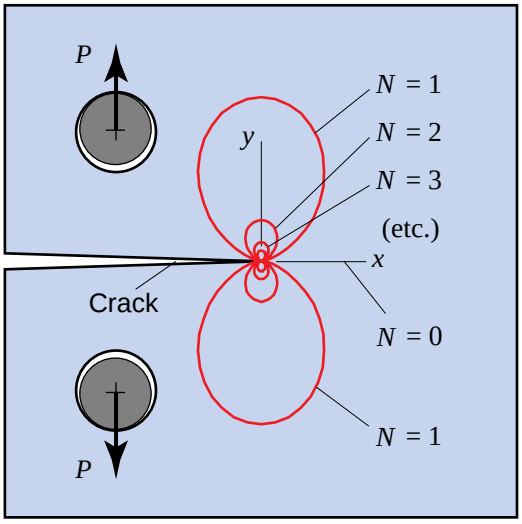

Fig. 35. Theoretical fringes for a K_I-dominant field.

We can now compare the theoretical fringe pattern with an actual fringe pattern from a photoelastic model (Fig. 36).[7] The features of the singular field are shown near the crack tip for values of N greater than about 4. Outside this region, however, the stress distribution is dominated by the

[7]Material, PSM-1. Load, 60 lb. Overall specimen size, 2.50 in. square, 0.213 in. thick; crack length a, 0.875 in., width w (Fig. 35), 2.00 in.

bending field and is also affected by the free boundaries of the specimen.

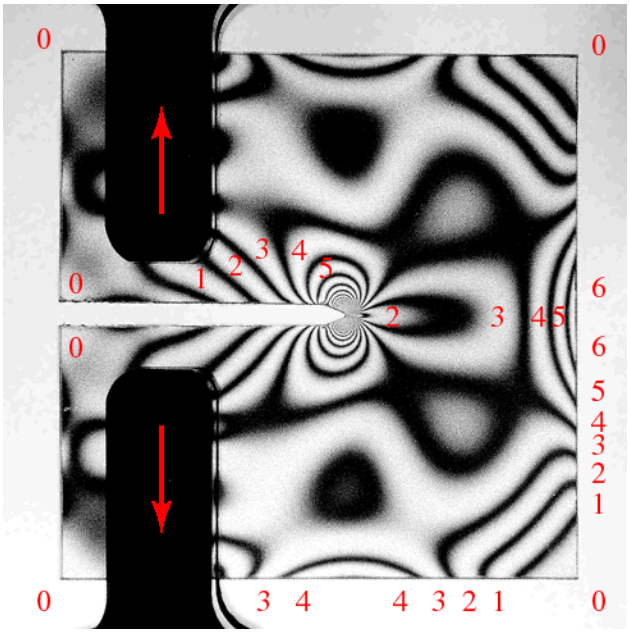

Fig. 36. Photoelastic model of a compact-tension specimen.

To compute the value of K_I for the specimen in Fig. 36, we first scale the photograph and determine that for the matching fringe loops of order $N = 5$, for example, the radius r at $\theta = \pm 90°$ is about 0.23 in. Therefore, from Eqn. (29),

$$K_I = \frac{\sqrt{2\pi r}\, f_\sigma N}{h} = \frac{\sqrt{2\pi(0.23)}(43)(5)}{0.213}$$
$$= 1.2 \text{ ksi}\sqrt{\text{in}}\,.$$

Meanwhile, according to Tada, Paris, and Irwin's *Stress Analysis of Cracks Handbook* (1973), the stress-intensity factor for this geometry and loading is given by

$$K_I = \frac{P}{h\sqrt{w}}\, f(\lambda), \qquad \lambda = \frac{a}{w},$$

where in this case (again from the photograph) a = 0.86 in. and w = 2.00 in., so that $\lambda = 0.43$. For this λ, $f(\lambda)$ is about 7.8. Therefore, K_I should have the value

$$K_I = \frac{60}{0.213\sqrt{2.00}}(7.8) = 1.55 \text{ ksi}\sqrt{\text{in}}\,.$$

The photoelastic analysis is seen to underpredict the value of K_I by about 25%, probably because the crack tip has a finite wedge angle and is rather

blunt. Dally and Riley (1991: Chapter 14) discuss various ways to improve K_I calculations from photoelastic data. One method, attributed to Schroedl, Smith, and others, results in a differencing equation (Eqn. (14.14) of Dally and Riley's text) that provides an improved estimate of about 1.4 ksi$\sqrt{\text{in}}$ if (in addition to the $N = 5$ data previously used) the radius r for the $N = 7$ fringe is taken to be about 0.13 in. The apparent underprediction is therefore reduced to about 8%, which would be marginally acceptable for most fracture-mechanics work.

Simulated photoelastic fringes

Considerable insight into the analysis of photoelastic fringes can be gained by constructing simulated fringes for known stress distributions.

Analytical

These constructions can be in the form of lines of constant N determined analytically, as in Fig. 35, where the solution $r(\theta)$ to Eqn. (29) is found explicitly, with N as a parameter.

Numerical—bitmap

Alternatively, a bitmap image can be constructed by calculating the intensity I numerically at each point in a large array of regularly spaced points, and by observing the resulting pattern. An example is shown in Fig. 37 for the dark-field isochromatics in a K_I stress field, based on Eqn. (29).

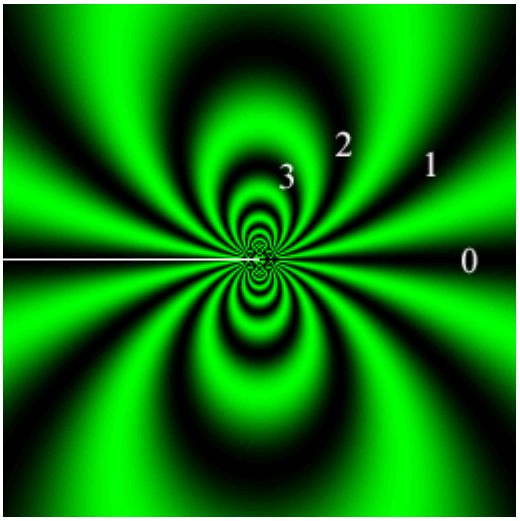

Fig. 37. Simulated K_I field (green light).

An advantage of this method is that it can be used even if the theoretical stress field is so complicated that it is impossible to determine the locus of constant N analytically.

The program used to generate the image in Fig. 37 is given below. The program was developed for arbitrary intensity and wavelength values of the colors red, blue, and green. A succession of separate bitmap files are created for steadily increasing load. The file format is BMP, which is the simplest of the standard image file types.

```
#include <windows.h>
#include <stdio.h>
#include <math.h>

// Windows-based C program for creating a color  BMP file
// of the photoelastic isochromatics for a KI field

// Matthew J Phillips and James W Phillips
// December 1997

// Pixel order is RGB for Mac, BGR for PC
typedef struct {
//   unsigned char red, green, blue;
     unsigned char blue, green, red;
} pixel;

// These image_* functions maintain the pixels for us:
typedef struct {
     int      width,
              height,
              rowbytes;
     char *imageptr;
} image;

image *image_new(int width, int height)

{
     image *pimNew;
     int rowbytes;

     rowbytes = sizeof(pixel)*width;
     // Make rowbytes a multiple of 4
     rowbytes = (rowbytes+3)&~3;

     pimNew = (image*)malloc(sizeof(image));
     pimNew->width = width;
     pimNew->height = height;
     pimNew->rowbytes = rowbytes;
     pimNew->imageptr = malloc(rowbytes*height);

     // Technically this isn't needed because we're going to
     // fill in the whole bitmap eventually, but just to be
     // nice ...

     memset(pimNew->imageptr,0xFF,rowbytes*height);

     return (pimNew);
}

void image_setpixel(image *pim, int x, int y, pixel *color)

{
     pixel *pixptr;

     pixptr = (pixel*)
         (pim->imageptr+pim->rowbytes*y+sizeof(pixel)*x);
     *pixptr = *color;
}

void image_writetofile(image *pim, FILE *fp)

{
     int y;

     for(y = 0; y < pim->height; y++) {
          fwrite(pim->imageptr+pim->rowbytes*y,
               1,pim->rowbytes,fp);
     }


}

void image_dispose(image *pim)

{
     free(pim->imageptr);
```

```
    free(pim);
}


// This function writes a Windows BMP file using the
// specified image as its source.

void write_BMP_file(image *pim, char *filename)

{
    BITMAPINFOHEADER bmi;
    BITMAPFILEHEADER fh;
    FILE *fp;

    fp = fopen(filename,"wb");

    fh.bfType = 'MB';
    fh.bfSize = sizeof(BITMAPFILEHEADER)
                        +sizeof(BITMAPINFOHEADER)
                        +pim->rowbytes*pim->height;
    fh.bfReserved1 = 0;
    fh.bfReserved2 = 0;
    fh.bfOffBits = sizeof(BITMAPFILEHEADER)
        +sizeof(BITMAPINFOHEADER);

    fwrite(&fh,1,sizeof(fh),fp);

   bmi.biSize = sizeof(BITMAPINFOHEADER);
   bmi.biWidth = pim->width;
   bmi.biHeight = pim->height;
   bmi.biPlanes = 1;
   bmi.biBitCount = 24;
   bmi.biCompression = BI_RGB;
   bmi.biSizeImage = 0;
   bmi.biXPelsPerMeter = 2835;
   bmi.biYPelsPerMeter = 2835;
   bmi.biClrUsed = 0;
   bmi.biClrImportant = 0;

    fwrite(&bmi,1,sizeof(bmi),fp);

    image_writetofile(pim,fp);

    fclose(fp);
}

typedef struct {
    double red, green, blue;
} dblpixel;

int main()

{
    image *pim;
    int px,py,n_pic;
    pixel c;
    double x,y,k,base_n;
    dblpixel intensity, wavelength, strength;
    char filenamebuf[32];

    float red, green, blue;


#define n_pics       10
#define k_max        1000.0
#define PI           3.14159265359
#define IMGWIDTH 256
#define IMGHEIGHT256

    printf("\r\nWavelengths (red, green, blue) (nm):  ");
    scanf ("%f %f %f", &red, &green, &blue);
    wavelength.red = red;
    wavelength.green = green;
    wavelength.blue = blue;
    printf("%f %f %f", wavelength.red,
        wavelength.green, wavelength.blue);

    printf("\r\nStrengths (red, green, blue) (0-255): ");
    scanf ("%f %f %f", &red, &green, &blue);
    strength.red = red;
    strength.green = green;
    strength.blue = blue;
    printf("%f %f %f", strength.red,
        strength.green, strength.blue);

    for(n_pic = 1; n_pic <= n_pics; n_pic++) {

        pim = image_new(IMGWIDTH,IMGHEIGHT);

        k = k_max*n_pic/n_pics;

        printf(
            "Generating image number %02d (k = %g).\r\n",
            n_pic,k);

        for(py = 0; py < IMGHEIGHT; py++) {
        //  y = ((double)py/(IMGHEIGHT-1))*2.0-1.0;
            y = ((double)py/IMGHEIGHT)*2.0-1.0;
            for(px = 0; px < IMGWIDTH; px++) {
                x = ((double)px/(IMGWIDTH-1))*2.0-1.0;
```

```
                // base_n is N(lambda) without
                // the 1/lambda factor
                if (x == 0.0 && y == 0.0) base_n = 0.0;
                else
                    base_n = k*fabs(y)/pow(x*x+y*y,3./4.);

                intensity.red = strength.red*
                    pow(sin(PI*base_n/wavelength.red),2);
                intensity.green = strength.green*
                    pow(sin(PI*base_n/wavelength.green),2;
                intensity.blue = strength.blue*
                    pow(sin(PI*base_n/wavelength.blue),2);

                c.red = (unsigned char)intensity.red;
                c.green = (unsigned char)intensity.green;
                c.blue = (unsigned char)intensity.blue;

                image_setpixel(pim,px,py,&c);
            }
        }

        // Overprint white crack

        c.red = 255;
        c.green = 255;
        c.blue = 255;

        y = 0.0;
        py = (int)(IMGHEIGHT/2*(y+1.0));
        for(px = 0; px < IMGWIDTH/2; px++) {
            image_setpixel(pim,px,py,&c);
        }

        sprintf(filenamebuf,"image_%02d.bmp",n_pic);
        write_BMP_file(pim, filenamebuf);
        image_dispose(pim);
    }
    return (0);
}
```

Note how the quantity $|\sin\theta|/\sqrt{r}$ is calculated in the code:

$$\frac{|\sin\theta|}{\sqrt{r}} = \frac{|y|}{r\sqrt{r}} = \frac{|y|}{r^{3/2}} = \frac{|y|}{\left(x^2+y^2\right)^{3/4}}.$$

This method is used to avoid trigonometric function calls and the problem of determining the correct inverse tangent of the angle θ corresponding to a given point (x,y).

Once the BMP files are created, they may be edited by a graphics program, such as Adobe Illustrator®, and saved in an alternative compressed format, such as Graphics Interchange Format (GIF). The fringe numbers that appear in Fig. 37 were added in this manner. An animated GIF can then be constructed using a program such as Microsoft GIF Animator®.

Numerical—Finite-element method

Finite-element codes, such as ABAQUS, have contour-plotting capabilities that allow various types of contours to be constructed so as to visualize the output.

If an option is available to plot the *in-plane* principal-stress difference, or, equivalently, twice the *in-plane* maximum shear stress, then this option can be used to generate simulated isochromatics.

A variable that is sometimes plotted to simulate photoelastic fringe patterns is the Tresca "equivalent stress" σ_{Tresca} given by

$$\begin{aligned}\sigma_{\text{Tresca}} &= 2\tau_{\max} \\ &= \max\left(|\sigma_1-\sigma_2|, |\sigma_2-\sigma_3|, |\sigma_3-\sigma_1|\right).\end{aligned}$$

In regions where the out-of-plane normal stress is an intermediate principal stress, the in-plane principal stress difference will in fact determine the value of σ_{Tresca}, and therefore a contour of constant σ_{Tresca} corresponds to an isochromatic of some order N. However, in regions where the out-of-plane normal stress is *not* intermediate, that is, it is either the minimum or maximum principal stress, the σ_{Tresca} contour will *not* coincide with an isochromatic.

As an example, consider the stresses in a curved beam due to pure bending (Fig. 38).[8] Only the curves for $R/h = 1$ are shown, but the observations we are about to make are independent of the value of R/h.

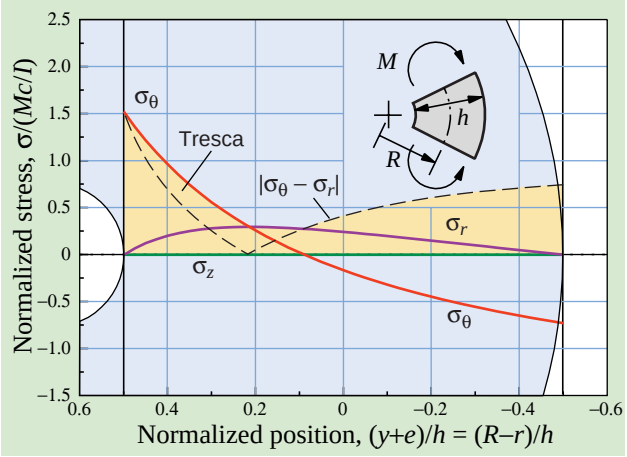

Fig. 38. Comparison of Tresca equivalent stress with in-plane principal-stress difference in a curved beam.

The hoop stress σ_θ varies from a positive value at the inside radius to a negative value at the outside radius. The radial stress σ_r vanishes at these extremes and reaches a maximum positive value near the center. If we let σ_1 and σ_2 denote the in-plane principal stresses, then

$$\sigma_1 - \sigma_2 = |\sigma_\theta - \sigma_r|,$$

[8]For a more complete discussion of the stresses in a curved beam, refer to the Appendix.

as shown with the dashed curve. It is this difference that would give rise to an isochromatic pattern. Note that the zero-order fringe is shifted considerably *towards* the center of curvature from the neutral axis, that is, from the point where the hoop stress σ_θ vanishes.

Meanwhile, the third principal stress σ_3, which is equal to the out-of-plane normal stress σ_z, has the value zero if we assume a state of plane stress. Wherever σ_3 is intermediate between σ_1 and σ_2, the Tresca equivalent stress and the difference $\sigma_1 - \sigma_2$ are the same thing—this is the situation for all of the section where σ_θ is compressive. However, near the center of the section, σ_θ becomes the intermediate principal stress and the Tresca equivalent stress is numerically equal to the radial stress σ_r since σ_z vanishes. Finally, near the inside radius, the radial stress σ_r becomes the intermediate principal stress, the hoop stress σ_θ dominates, and the Tresca equivalent stress becomes numerically equal to the hoop stress because, again, σ_z vanishes.

In this simple example, it is seen that the Tresca equivalent stress and the in-plane principal stress difference can be, but are often not, the same thing. One can expect that in more complicated shapes analyzed by the finite-element method, the matching of these two quantities would need to be checked carefully.

Photoelastic photography

Next we consider some practical aspects of observing and recording photoelastic fringe patterns.

Collimated vs. diffuse light

One choice to be made is whether the light that traverses the specimen is *collimated*. In the traditional optical arrangement (Fig. 39), the light source produces diverging light from a tiny aperture, and a large field lens placed at is focal length from this source produces collimated light that is passed through all the polariscope elements and is collected by a second large field lens.

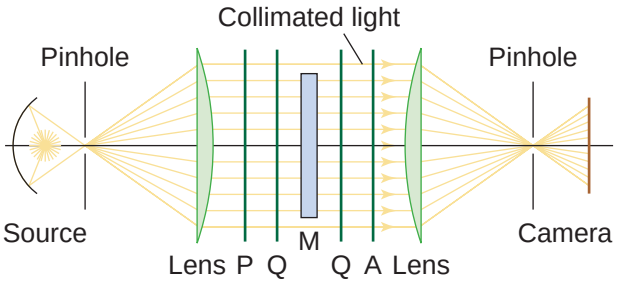

Fig. 39. Collimated light source.

A pinhole placed at the focal point of the second field lens eliminates stray light and allows a real image of the specimen to form on a piece of paper or photographic film. Smaller pinholes produce sharper images of reduced intensity.

The light source can be a specially designed mercury-vapor or incandescent lamp in a housing having various-sized pinhole openings, or it can be a laser beam passed through an expanding lens.

This arrangement has the advantage that the edges of the specimen are in sharp focus, since the collimated light propagates parallel to these edges. Also, no focusing is required. Disadvantages include the cost of the large field lenses, and the fact that *all* the optical elements in the region of collimated light are in focus; therefore all imperfections (such as scratches and dust) appear in sharp focus in the recorded image. Also, rather large film sizes (such as 5x7-in.) are required for good image reproduction.

An alternative arrangement that allows the use of an ordinary 35 mm film camera or a CCD video camera employs a *diffuse* light source (Fig. 40). A ground glass or other translucent material is placed between the light source (which need not be a pinhole type) and the other optical elements. Every point on this diffusing surface produces light that propagates in all directions.

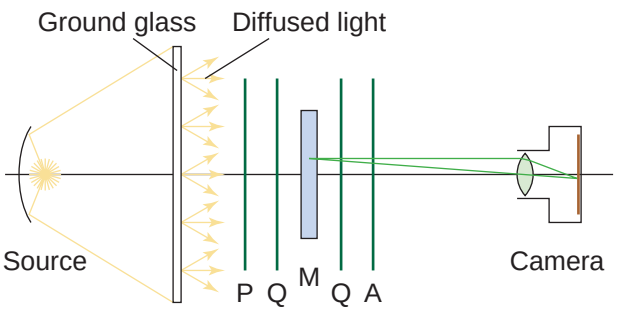

Fig. 40. Diffuse light source.

One of the advantages of this method is that an ordinary camera can be used—and with 1-hour photo finishing being commonplace today, this fact alone makes the arrangement attractive. (Alternatively, a video camera can be used to record the image "live" or allow a frame-grabber to acquire a sequence of fringe patterns.) Another advantage is that this arrangement is generally more compact than the collimated one.

The principal disadvantage is that the light is no longer passing parallel to the specimen edges and therefore the edges do not appear sharp. This parallax problem can be reduced by moving the camera farther away from the specimen, but then the image size is reduced. A long focal-length lens will help, but then focusing becomes critical.

White vs. monochromatic light

A quite separate issue is whether the light used is *white* (that is, rich in many colors) or is *monocromatic*. There are advantages and disadvantages to either type.

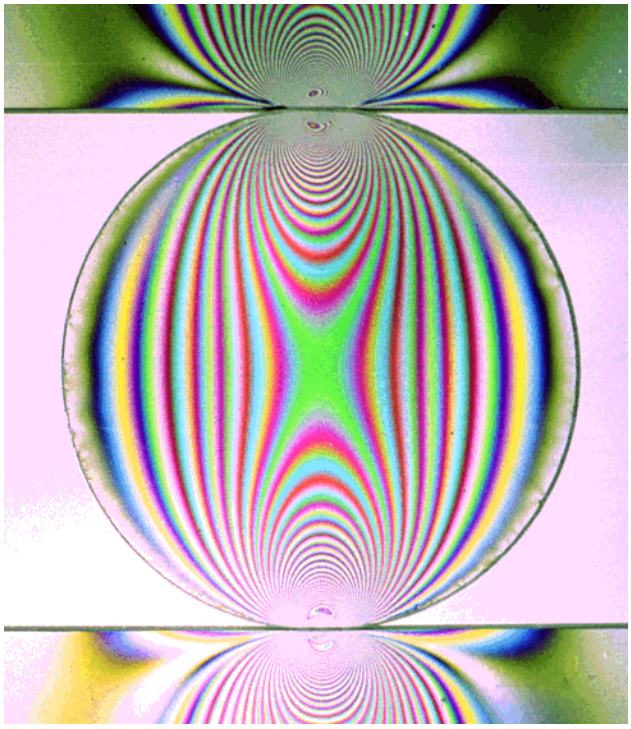

Fig. 41. Approximate white-light light-field isochromatics for a disk in diametral compression.

Consider the fringe pattern in a circular disk loaded in diametral compression between photo-

elastic strips of the same material, and photographed using white light (Fig. 41).[9]

The image is striking but is difficult to analyze because the colors interfere. Now compare this figure with that in Fig. 42, which is for the *same* specimen at the *same* load with the *same* light source, but with a Tiffen® #58 dark green filter placed over the camera lens.

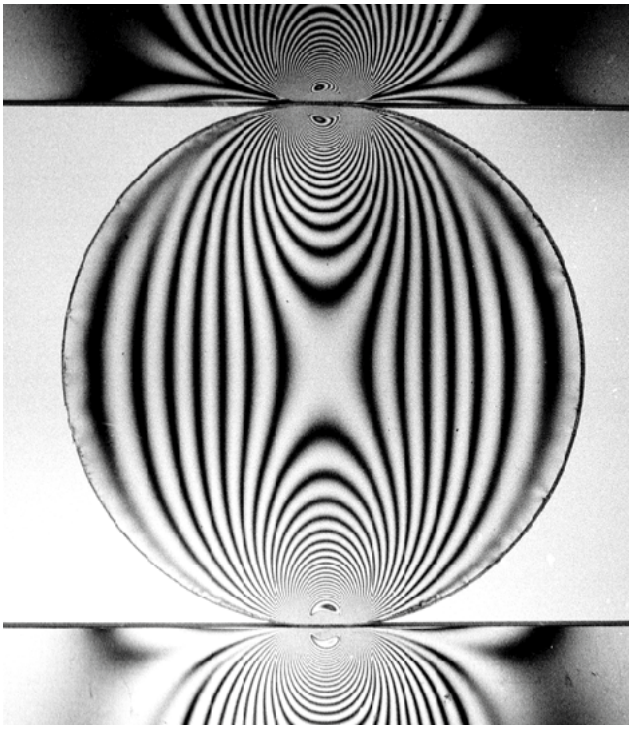

Fig. 42. Filtered green-light light-field isochromatics for a disk in diametral compression.

Observe that a *light* fringe of order $N = 7$ is at the center of the disk when approximately monochromatic green light is used. Now refer back to Fig. 41 and observe that the center of the disk has a *green* fringe. Apparently at this point, the red and blue components have low intensity, allowing green to dominate.

To see why isochromatics are so colorful when viewed in white light, consider the *absolute* retardation given by Eqn. (6):

$$\delta = hc(\sigma_1 - \sigma_2),$$

[9]Material, PSM-1. Load, 298 lb. Diameter, 2.489 in. Light source, mercury vapor. Blue and red components artificially enhanced to simulate a white-light source.

where c is the relative stress-optic coefficient. The value of c is independent of wavelength, and therefore δ is a function only of the stress difference $\sigma_1 - \sigma_2$. However, when the retardation δ is expressed as a fraction of the light wavelength λ, so as to determine the number of cycles N of *relative* retardation

$$N = \frac{\delta}{\lambda},$$

the value of N is seen to vary inversely as the wavelength. It is the value of N, and not δ, that determines the intensity of light at a given point in the specimen. For example, in a dark field (circular polariscope), the intensity varies as

$$I = a^2 \sin^2 \frac{\Delta}{2} = a^2 \sin^2 \pi N$$
$$= a^2 \sin^2 \pi \frac{\delta}{\lambda}.$$

If we decompose white light into the primary colors red, green, blue (RGB) and examine the dependence of I on δ for the representative wavelengths, say

$$\lambda_{\text{red}} = 650 \text{ nm},$$
$$\lambda_{\text{green}} = 550 \text{ nm},$$
$$\lambda_{\text{blue}} = 450 \text{ nm},$$

then we obtain the results shown in Fig. 43.

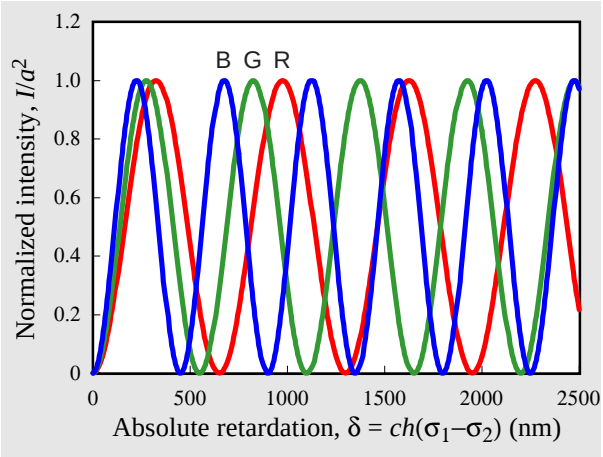

Fig. 43. Dark-field intensity variations for representative primary-color wavelengths.

With the important exception of $\delta = 0$, we observe that the value of δ that causes the intensity of a given color to vanish generally does *not* cause

the intensity of the other two colors to vanish, and therefore some combination of the other two colors will be visible. We conclude that in a dark-field polariscope (plane or circular), *only the zero-order isochromatic is black*. All other isochromatics have locations that depend on the wavelength.

In a light-field polariscope (which *must* be circular), the situation is similar, except now the intensity varies as the cosine squared instead of the sine squared:

$$I = a^2 \cos^2 \frac{\Delta}{2} = a^2 \cos^2 \pi N$$
$$= a^2 \cos^2 \pi \frac{\delta}{\lambda}.$$

The corresponding results are shown in Fig. 44.

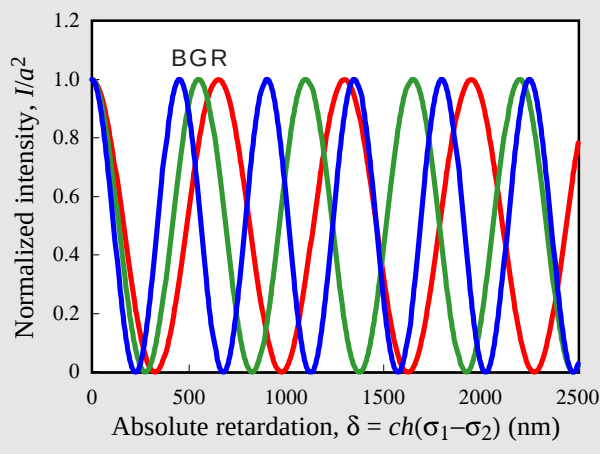

Fig. 44. Light-field intensity variations for representative primary-color wavelengths.

In this figure we see that there really is *no* location where the intensity vanishes for *all* colors. Instead, for $\delta = 0$, the intensity is a maximum for all colors and therefore *the zero-order isochromatic appears light*. The $\frac{1}{2}$-order fringe has the narrowest range of δ for which the intensities are minimal and therefore is the "blackest" of the isochromatics.

Note that the order of colors in an isochromatic pattern is well defined. As δ increases, the *relative* retardation for blue light outpaces that of green and red because blue light has the *shortest* wavelength. Therefore, regardless of the field (dark or light), blue fringes appear ahead of green and red fringes. Sometimes an individual primary color is seen distinctly, but this condition requires that the other

two components vanish, and such a condition is rare. As a consequence, the fringe pattern consists of continuously varying colors, *not* bands of primary colors. Blue and green, for instance, combine to form a blue–green called cyan, green and red combine to form yellow, and red and blue combine to form magenta. All three combine to form white. The first-order "light" fringe in a light-field pattern (Fig. 44) is really a band of colors consisting of black–blue–cyan–green–yellow–red–magenta, followed by a strong blue and a strong green. These features can be seen in the diametrally loaded disk (Fig. 41) near the outside edge. Observe, for instance, the strong yellow band, where blue is reaching a relative retardation of $1\frac{1}{2}$ cycles and is therefore vanishing, leaving green and red to combine and form yellow.

Further insight is gained by decomposing an unfiltered mercury-vapor light-source isochromatic pattern into its component RGB colors (Fig. 45). The decomposition is achieved electronically from the scanned negative.

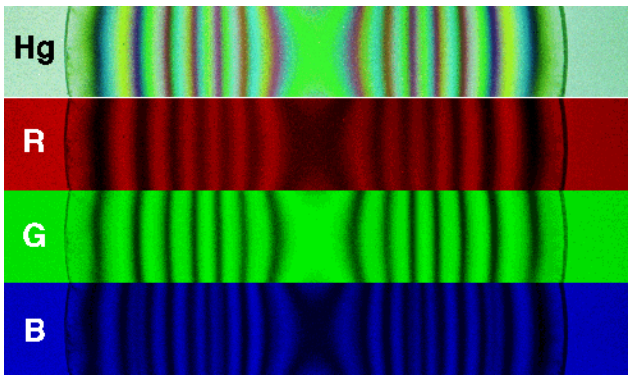

Fig. 45. Central band of a disk in diametral compression in its original form (Hg) and decomposed into its RGB components.

At the center of the disk, the green fringe of order 7 is seen to correspond to the red fringe of order 6.5 and to the blue fringe of order 9.5. Now, if the characteristic wavelength of green light is taken to be 550 nm, the absolute retardation δ at the center of the disk must be

$$\delta = N_{\text{green}}\lambda_{\text{green}} = 7.0(550\text{ nm})$$
$$= 3850\text{ nm}\,.$$

If red light is observed to produce a fringe order of 6.5 at the same point, then the characteristic wavelength of this light must be

$$\lambda_{\text{red}} = \frac{\delta}{N_{\text{red}}} = \frac{3850\ \text{nm}}{6.5} = 590\ \text{nm}\,.$$

Similarly, if blue light is observed to produce a fringe order of 9.5 at the same point, then the characteristic wavelength of this light must be

$$\lambda_{\text{blue}} = \frac{\delta}{N_{\text{blue}}} = \frac{3850\ \text{nm}}{9.5} = 400\ \text{nm}\,.$$

It should be emphasized that a mercury light source has many lines in its spectrum, and the effects observed here are weighted averages of the strengths of these lines, the spectral sensitivity of the color film, and the spectral sensitivities of the red, green, and blue sensors in the film scanner. Nevertheless, it is remarkable that the wavelength separation between blue and green is observed to be much larger than that between green and red.

The beautiful rainbow colors of the white-light isochromatics are fascinating but they complicate the data analysis, particularly for high-order fringes, which tend to "wash out" because the almost random combinations of the primary colors virtually guarantee that light of *some* wavelength will not be extinguished. This problem is particularly acute if the *recording* system responds in a panchromatic fashion (that is, to all colors of light), but records the image in monochromatic form (as, for example, a black-and-white CCD camera or black-and-white film). For the sharpest fringe recording, monochromatic light is preferred.

There are advantages to the white-light source, however. In a plane polariscope, the isochromatics are brightly colored while the isoclinics are black; therefore the two patterns are easily distinguished in the laboratory or in a color photograph, whereas they would not be easily distinguished if monochromatic light were used.

Also, in a dark-field (plane or circular) polariscope, *only the zero-order isochromatic fringe is black* and therefore this important fringe order can be distinguished from all the higher-order ones; the same cannot be said if the light source is monochromatic. To see this effect, compare the white-light simulated isochromatics for a K_{I} field

(Fig. 46) with those using a monochromatic light source (Fig. 37).

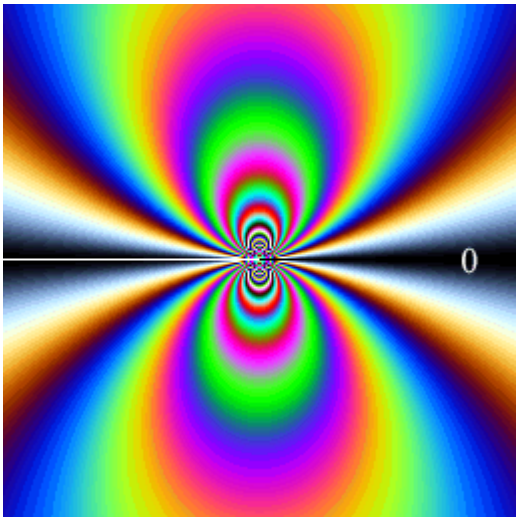

Fig. 46. Simulated K_I field (white light).

Similarly, in a light-field (circular) polariscope, the $\frac{1}{2}$-order isochromatic fringe is the "blackest" of the dark fringes—observe the color intensities in Fig. 44 for retardations in the range of 250 nm. The fringe pattern in Fig. 41 illustrates this point well.

Compensation

The term *compensation* refers to any technique used to determine fractional fringe orders.

Interpolation and extrapolation

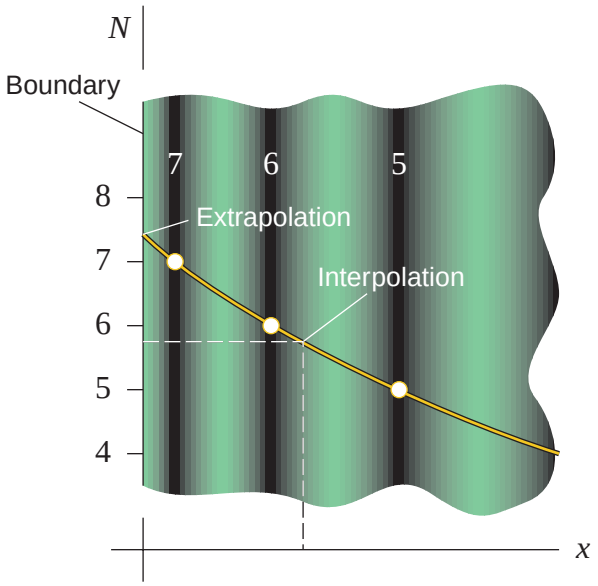

Fig. 47. Interpolation and extrapolation.

The simplest compensation techniques are *interpolation* and *extrapolation* of data based on whole-order (and/or half-order) fringe locations (Fig. 47).

Interpolation is the more reliable of these methods but it is necessarily restricted to interior points in the specimen.

Extrapolation is the less reliable method but is required if fractional values of N are to be determined along the boundary of the specimen. This method is less reliable than interpolation for two reasons:

- It requires a guess of the proper analytical approximation *outside* the domain in which such an approximation can be deduced on the basis of known points.
- It is subject to errors in fringe values near the surface. Such errors may be due to surface imperfections or to residual heat- or moisture-induced birefringence that has nothing to do with the applied stresses. Residual edge stresses appear in an unloaded specimen; they cause a characteristic sudden turning of obliquely intersecting isochromatics at the edge, and a local shift of near-edge isochromatics that are parallel to the edge.

Since the maximum stresses (which are usually the stresses of primary interest) often occur at the boundary, it behooves the specimen fabricator to prepare the surface with as much care as possible, leaving it nick-free and devoid of heat-induced residual fringes.

Tardy compensation

A technique that takes the guesswork out of determining fractional fringe orders is Tardy compensation. It works equally well for interior and boundary points, although for boundary points it is adversely affected by heat- or moisture-induced residual stresses. The method requires 3 steps for every point analyzed:

1. The polarizing directions of the polarizer and analyzer are aligned with the principal-stress directions at the point. This step is accomplished by using a *plane* polariscope and by rotating the polarizer and analyzer together until an isoclinic passes through the point, thereby leaving

$$\alpha = 0 .$$

2. The polariscope is converted from plane to circular by rotating the quarter-wave plates to their 45° orientations with respect to the polarizer and analyzer. The polarizer and analyzer are held fixed during the conversion, leaving the polariscope in the dark-field circular configuration, still with $\alpha = 0$, but with no isoclinics.

3. The analyzer *alone* is rotated through some angle γ, as shown in Fig. 48, until a neighboring (dark) isochromatic of *integer* order *n* passes through the point in question.

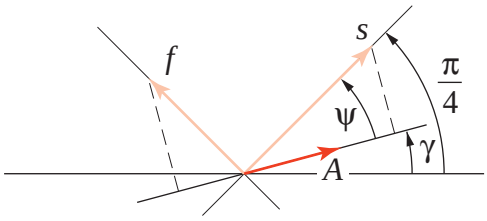

Fig. 48. Light leaving the analyzer (Tardy compensation).

The fractional fringe order is then equal to the ratio γ / π, as will be shown subsequently. Therefore the value of *N* at the point is

$$N = n \pm \frac{\gamma}{\pi} . \qquad (30)$$

The sign of the fractional correction depends on the orientation of the quarter-wave plates. For CCW rotating light, the + sign applies, and for CW rotating light, the – sign applies.

To derive Eqn. (30), we start with the expressions for the slow and fast wave amplitudes *s* and *f*, respectively, that leave the second quarter-wave plate in a circular polariscope. Since $\alpha = 0$, the angle ϕ has the special value $\phi = \frac{\pi}{4} - \alpha = \frac{\pi}{4}$; therefore, from Eqns. (17),

$$
\begin{aligned}
s &= \frac{P}{\sqrt{2}} e^{-i\pi/4}\left(i\cos\frac{\pi}{4} - e^{i\Delta}\sin\frac{\pi}{4}\right) \\
&= \frac{P}{2} e^{-i\pi/4}\left(i - e^{i\Delta}\right), \\
f &= \frac{P}{\sqrt{2}} e^{-i\pi/4}\left(-\sin\frac{\pi}{4} + ie^{i\Delta}\cos\frac{\pi}{4}\right) \\
&= \frac{P}{2} e^{-i\pi/4}\left(-1 + ie^{i\Delta}\right).
\end{aligned}
$$

From Fig. 48, the amplitude A of light leaving the analyzer is given by

$$A = s\cos\psi - f\sin\psi,$$

where the angle $\psi = \frac{\pi}{4} - \gamma$ is introduced for convenience:

$$
\begin{aligned}
A &= s\cos\psi - f\sin\psi \\
&= \frac{P}{2} e^{-i\pi/4}\left[\left(i - e^{i\Delta}\right)\cos\psi - \left(-1 + ie^{i\Delta}\right)\sin\psi\right] \\
&= \frac{P}{2} e^{-i\pi/4}\left[i\cos\psi + \sin\psi - e^{i\Delta}(\cos\psi + i\sin\psi)\right] \\
&= \frac{P}{2} e^{-i\pi/4}\left[i(\cos\psi - i\sin\psi) - e^{i\Delta}(\cos\psi + i\sin\psi)\right] \\
&= \frac{P}{2} e^{-i\pi/4}\left[e^{i(\pi/2-\psi)} - e^{i(\Delta+\psi)}\right] \\
&= \frac{P}{2} e^{-i\pi/4} e^{i(\pi/2-\psi+\Delta+\psi)/2}\cdot 2i\sin\left(\frac{1}{2}\left(\frac{\pi}{2} - \psi - \Delta - \psi\right)\right) \\
&= Pe^{i\Delta} e^{i\pi/2}\sin\left(\frac{\pi}{4} - \psi - \frac{\Delta}{2}\right).
\end{aligned}
$$

Since $P = ae^{i\Phi}$ and $\frac{\pi}{4} - \psi = \gamma$, the magnitude of A is simply

$$|A| = a\sin\left(\gamma - \frac{\Delta}{2}\right),$$

and therefore the intensity I of light leaving the analyzer is

$$I = |A|^2 = a^2\sin^2\left(\gamma - \frac{\Delta}{2}\right). \qquad (31)$$

This light intensity vanishes wherever $\gamma - \frac{\Delta}{2}$ is equal to $-n\pi$, where n is an integer. Solving for the relative angular retardation Δ and dividing it by 2π gives

$$N = \frac{\Delta}{2\pi} = n + \frac{\gamma}{\pi}. \qquad (32a)$$

The sign of the γ / π term is correct for counter-clockwise rotating circularly polarized light passing through the specimen (Fig. 21). If the slow and fast axes of the quarter-wave plates are reversed, then the circularly polarized light passing through the specimen will rotate clockwise, and it can be shown that

$$N = \frac{\Delta}{2\pi} = n - \frac{\gamma}{\pi}. \qquad (32b)$$

In practice, the sign of the correction is determined by first interpolating visually to obtain an estimate of the fractional fringe order (with the analyzer and polarizer crossed), then by rotating the analyzer until the closest whole-order fringe moves to the point.

Typically, the value of γ can be resolved to within 2^o, so the fractional part γ / π can be resolved to within $2^o/180^o$ or about 0.01. If the value of N is considerably smaller than 1, the *relative* error in N can be appreciable, but if N is of order 1 or more, then the *relative* error in N is less than 1%, which is quite acceptable.

Separation

The term *separation* refers to any technique for determining one of the principal stresses uniquely. It must be remembered that when we use the basic relation

$$\sigma_1 - \sigma_2 = \frac{N f_\sigma}{h},$$

we determine only the *difference* between the principal stresses—not these stresses separately.

Boundary condition

Perhaps the most important separation method consists of applying the boundary condition at a free edge of the specimen (Fig. 49). If t and n denote the tangential and normal directions at a free boundary, then $\tau_{nt} = 0$ because there is no shear traction applied at the boundary, and therefore the normal stresses σ_n and σ_t are principal stresses.

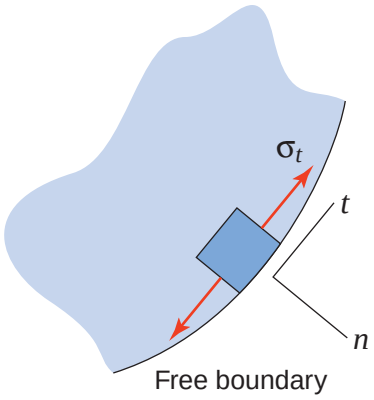

Fig. 49. Stress state at a free boundary.

Furthermore, $\sigma_n = 0$ because there is no normal traction applied to the surface, either. The principal stresses are now separated because one of them, σ_n, is equal to zero and the other one, σ_t, must account for the difference $\sigma_1 - \sigma_2$:

$$\begin{aligned} \sigma_n &= 0\,, \\ \sigma_1 - \sigma_2 &= |\sigma_t| = \frac{N f_\sigma}{h}\,. \end{aligned} \tag{33}$$

Note that the *sign* of the tangential normal stress is not resolved; it may be positive, negative, or zero.

As an example of the application of this separation technique, consider the U-shaped specimen in bending (Fig. 50).[10] *All* of the visible boundary is a free boundary and therefore the normal stresses may be separated anywhere along this boundary.

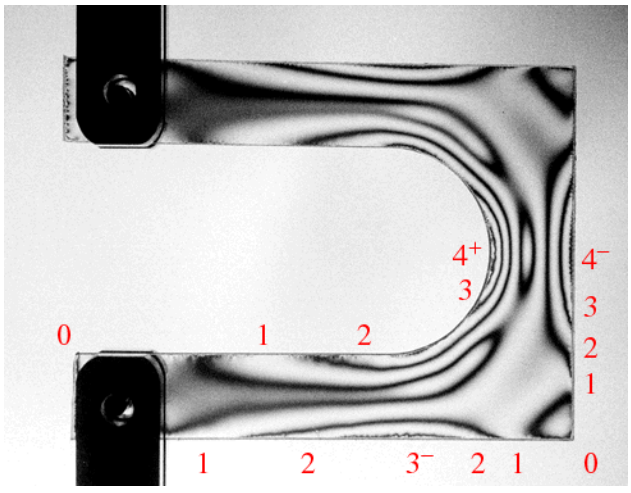

Fig. 50. Light-field isochromatics in a U-shaped specimen subjected to an opening load.

[10]Material, PSM-1. Load, approximately 3 lb. Thickness, 0.213 in.

In particular, at the inside curvature, the maximum tangential stress is known to be positive. Since by extrapolation N is approximately 4.2 at this point, we have

$$\sigma_n = 0,$$
$$|\sigma_t| = \sigma_t = \frac{4.5(43)}{0.213} = 910 \text{ psi}.$$

At the outside straight edge, N is approximately 3.8, and the tangential stress is known to be negative. Therefore,

$$\sigma_n = 0,$$
$$|\sigma_t| = -\sigma_t = \frac{3.8(43)}{0.213} = 770 \text{ psi},$$

that is, $\sigma_t = -770$ psi.

The fact that the principal stresses are easily separated along a free boundary led to the early use of photoelasticity to determine stress-concentration factors for cutouts, fillets, holes, etc., in a wide variety of geometrical shapes subjected to different loads. The technique is applicable to both static and dynamic photoelastic investigations.

Caution. The technique applies only to a free boundary. It does not hold at contact points, where the normal stress σ_n becomes large; and it does not hold for interior points. One might be tempted, for example, to extend the principle to all points along the plane of symmetry of the model in Fig. 50, arguing that τ_{xy} vanishes along the plane of symmetry, and that σ_x is equal to zero at the left- and right-hand ends; therefore σ_x must be equal to zero everywhere along the symmetry plane. But σ_x does *not* vanish along the symmetry plane if at least one of the surfaces is curved, as can be seen by an equilibrium argument that is used, in fact, to derive an expression for the radial stress component in a curved beam in bending.[11]

Shear-difference method

To separate the principal stresses in the interior of a specimen, more work is required. A method that is particularly useful because it does not require any additional experimental apparatus is the *shear-*

[11]See the Appendix.

difference method, which is based on stress equilibrium, as will be shown subsequently.

Before we examine this method, let us first observe what can be determined easily at *any* point in the specimen using a combination of isochromatics and isoclinics. The isochromatics provide the principal-stress difference

$$\sigma_1 - \sigma_2 = \frac{Nf_\sigma}{h}$$

and therefore the radius R of Mohr's circle

$$R = \frac{\sigma_1 - \sigma_2}{2} = \frac{Nf_\sigma}{2h}, \tag{34}$$

as shown in Fig. 51.

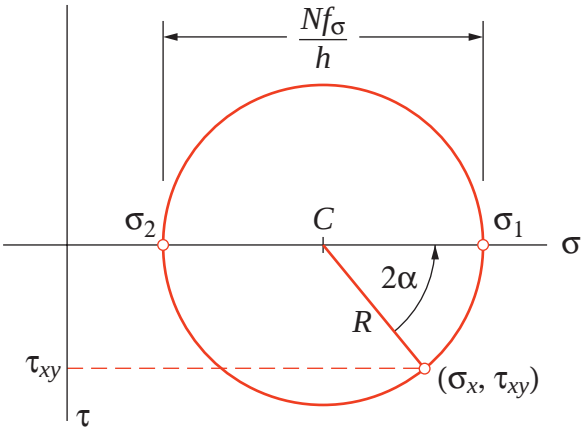

Fig. 51. Calculation of τ_{xy} from isochromatics and isoclinics at an arbitrary point.

Meanwhile, a complete family of isoclinics will provide values of the principal-stress orientation α throughout the specimen. (Examples of isoclinics are given in Fig. 52[12] for the disk in diametral compression.) Thus, at any point in the specimen, the angle 2α in Mohr's circle can be found.

Observe from Fig. 51 that the shear stress τ_{xy} has the value

$$\tau_{xy} = R\sin 2\alpha = \frac{Nf_\sigma}{2h}\sin 2\alpha \tag{35}$$

and that sufficient information is available from the isochromatics and isoclinics to determine this value anywhere in the specimen.

[12]Material, PSM-1. Load, 128 lb. Diameter, approximately 2.5 in. Light source, mercury vapor, unfiltered.

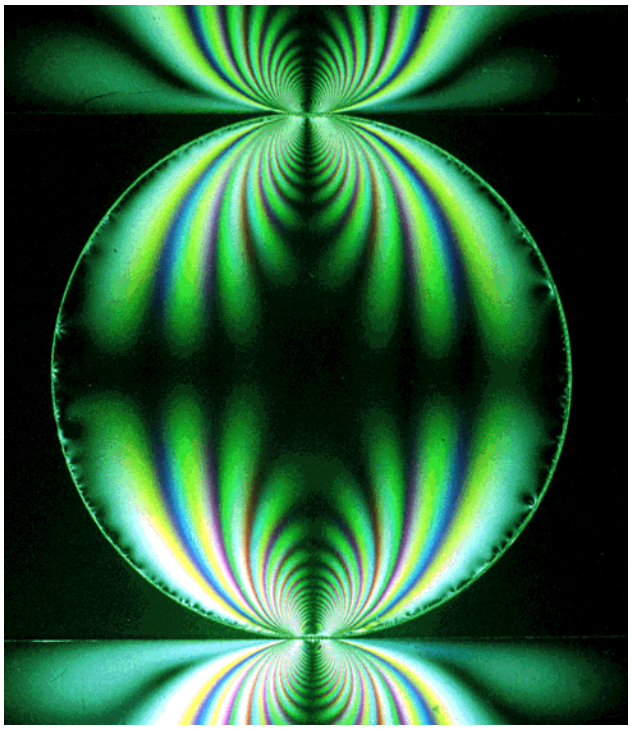

Fig. 52(a). The 0º/90º isoclinics for a disk in diametral compression.

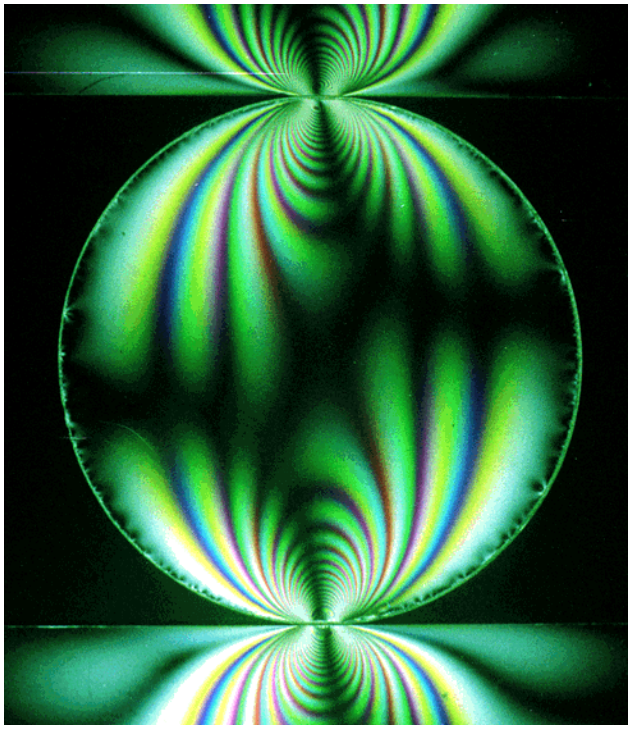

Fig. 52(b). The 10º/100º isoclinics for a disk in diametral compression.

We now consider how to use values of τ_{xy} along certain lines in the specimen to separate the principal stresses. Recall from stress equilibrium (Fig. 53) that, in the absence of body forces,

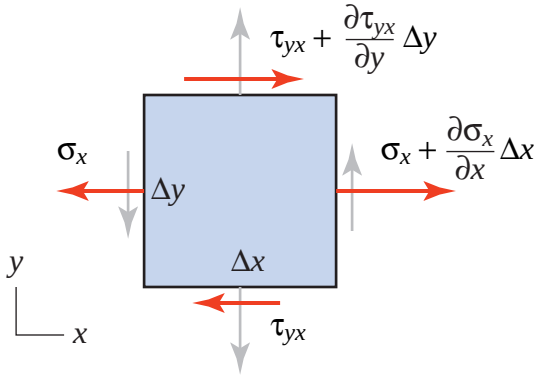

Fig. 53. Differential stress element.

$$\frac{\partial \sigma_x}{\partial x} + \frac{\partial \tau_{xy}}{\partial y} = 0$$

everywhere in the body. Along a line y = const (Fig. 54), $dy = 0$, and therefore

$$\begin{aligned} d\sigma_x &= \frac{\partial \sigma_x}{\partial x} dx + \frac{\partial \sigma_x}{\partial y} dy \\ &= -\frac{\partial \tau_{xy}}{\partial y} dx + \frac{\partial \sigma_x}{\partial y} \cdot 0 \\ &= -\frac{\partial \tau_{xy}}{\partial y} dx \,. \end{aligned} \tag{36}$$

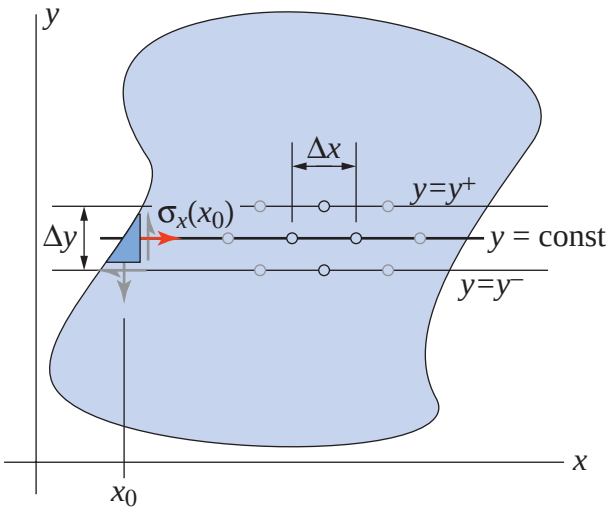

Fig. 54. Integration path for the shear-difference method.

In the shear-difference method, we write the central-difference approximation for $\partial \tau_{xy} / \partial y$ as

$$\frac{\partial \tau_{xy}}{\partial y} \cong \frac{\tau_{xy}^+ - \tau_{xy}^-}{\Delta y},$$

where $\tau_{xy}^{+}(x)$ and $\tau_{xy}^{-}(x)$ denote the values of shear stress along the lines $y = y^{+}$ and $y = y^{-}$, respectively, and then integrate Eqn. (36) from $x = x_0$ to an arbitrary point x along the line y = const:

$$\sigma_x(x) - \sigma_x(x_0) = -\int_{x_0}^{x} \frac{\tau_{xy}^{+} - \tau_{xy}^{-}}{\Delta y}\, dx' . \quad (37)$$

This is the *shear-difference formula* for finding the value of σ_x anywhere along the line y = const. With σ_x known at a point, all the normal stresses can be found at that point because the center C of Mohr's circle is located at

$$C = \sigma_x - R\cos 2\alpha ,$$

and with C known, the entire Mohr's circle can be constructed.

The initial value $\sigma_x(x_0)$ in general must be found by using a Mohr's circle construction after the principal stresses have been separated at $x = x_0$ using the traction-free boundary condition there.

The shear-difference formula is often written directly in terms of isochromatic and isoclinic data. Recalling that $\tau_{xy} = R\sin 2\alpha$, where $R = \frac{Nf_\sigma}{2h}$, we find that

$$\sigma_x(x) = \sigma_x(x_0) - \frac{f_\sigma}{2h\Delta y} \times \int_{x_0}^{x} \left(N^{+} \sin 2\alpha^{+} - N^{-} \sin 2\alpha^{-} \right) dx' . \quad (38)$$

To avoid error propagation, it is a good idea to plot smoothed curves through the data for $N^{+}\sin 2\alpha^{+}$ and $N^{-}\sin 2\alpha^{-}$, then to use a high-order integration scheme, such as Simpson's rule, to carry out the integration of the difference between these terms.

Photoelastic coatings

We close the discussion of photoelasticity with an important application that permits surface analysis of actual components that have irregular surfaces.

A photoelastic coating can be molded to the surface contour of a complicated part and bonded to it (Fig. 55). Light is reflected at the coating–component interface and therefore propagates twice

through the coating thickness h, giving an effective path length of $2h$ in the coating.

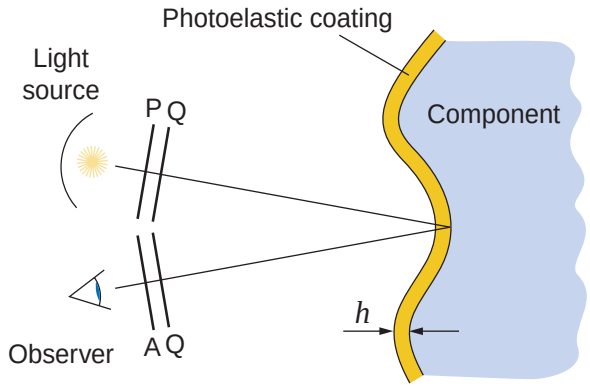

Fig. 55. Photoelastic coating.

The component is now the primary load-carrying member, not the photoelastic material. The in-plane coating strains are assumed to be equal to the in-plane surface strains in the component, and the analysis of the photoelastic patterns is based on the principal *strain* difference, which is related to the principal *stress* difference in the component through the elastic constants of the component material. In this respect, photoelastic coatings are regarded in much the same way as brittle coatings.

As discussed in Dally and Riley (1991), compromises must be made. For example, the coating must be thick enough to generate a reasonable number of fringes in response to the component strains, yet not so thick that the average strains in the coating deviate significantly from the interface strains and the coating begins to reinforce the component.

For components that undergo very small strains when loaded, very sensitive coatings must be used, and a careful analysis of the colors of the isochromatics may be needed to determine fractional fringe orders.

References

Dally, J. W., and W. F. Riley. 1991. *Experimental Stress Analysis*, 3rd ed. New York: McGraw-Hill.

Tada, H., P. C. Paris, and G. R. Irwin. 1985. *Stress Analysis of Cracks Handbook*, 2nd ed. St. Louis, Mo.: Paris Productions, Inc.